Developing a CFD-based axial compartment model for a lab scale bioreactor

by

Blake A. Karawan

B.S., University of Charleston West Virginia, 2013
B.S., West Virginia University Institute of Technology, 2019

A REPORT

submitted in partial fulfillment of the requirements for the degree

MASTER OF SCIENCE

Department of Chemical Engineering
Carl R. Ice College of Engineering

KANSAS STATE UNIVERSITY
Manhattan, Kansas

2022

Approved by:

Major Professor
Dr. Davood Pourkargar

Copyright

Abstract

Processes involving biological reactions are essential for modern society. Food additives, pharmaceuticals, and commodity chemicals are all major industries that utilize cellular activity to generate desired materials. From penicillin to citric acid, products of bioreactors touch many aspects of day to day life. Accurate models are invaluable to minimize the time and cost associated with process design, scale-up, control, and optimization. However, bioreactors provide unique challenges for the development of accurate yet computationally efficient models due to sensitivity to small changes across different time and length scales. Ultra-high-fidelity modeling using computational flow dynamics (CFD) is too computationally expensive for versatile bioreactor modeling, while simple ideal models do not account for how the flow field affects reactor performance. A compartment model (CM) offers the best of both worlds; by sacrificing some resolution, flow dynamics can be incorporated into a fast-solving model. These models show promise in accurate prediction with short computation times, and the resolution can be adjusted depending on the desired modeling application. CMs are generated based on flow information derived either from experimentation or CFD modeling. A sampling of CM approaches is presented in this work. Additionally, a case study is presented, in which an empirical compartment modeling approach is adapted for use with CFD output. The developed one-dimensional axial CM showed good agreement with the CFD model for mixing times from a simulated concentration step change, although a loss of predictive ability was observed with rigorously modeled acid injection. The results indicate that, with minor modification to the compartmental framework, the developed CFD-CM can be made more accurate while remaining computationally inexpensive.

Table of Contents

List of Figures

List of Tables

Acknowledgements

First and foremost, I would like to thank my wife, Christi. Without her steadfast support (and the occasional threats of handcuffing me to my desk in the face of looming deadlines) this journey would never have been possible.

Dr. Davood Pourkargar, for his mentorship and guidance throughout the entirety of the project. His excitement and willingness to have in-depth and lengthy discussions about our ideas was a much-appreciated source of incredible inspiration to drive the project to completion.

Thiago Oliveira Cabral, the developer of the CFD model often referenced in this work. Without his technical proficiency or his willingness to generate data and share his own insights, this work would not have been possible.

My committee members, Dr.'s Placidus Amama and John Schlup, for their time, guidance, and insights to help me create the best version of this work.

Last but in no way least, my grandpa, Al Skinner, who continually keeps my spirits up and finds ways to inspire me to always reach just a little further to achieve my dreams.

Introduction

Bioreactors cultivate living cells to take advantage of natural processes that produce various useful materials. Products that rely on biochemical processes are ubiquitous throughout modern society with examples including commodity chemicals (such as alcohols or ketones), food additives (such as citric acid, lactic acid, high fructose corn syrup, or baker's yeast), medicines (such as penicillin or anti-cancer drugs), bio-based monomers and polymers, and renewable fuel sources [1] [2]. Bioethanol production alone has an annual production of 80 million tons [2]. Reliable operation and design of bioprocesses, therefore, is essential for humanity. As a result, the development of an accurate yet user-friendly model is essential. Among other things, accurate simulations can aid in the design and scale-up of processes or in predicting how a bioreactor may respond to changing conditions. However, bioreactors provide unique challenges for the development of accurate, yet computationally efficient, models. For example, as systems get larger, small details unimportant at the lab scale can drastically change the performance of a manufacturing scale operation [1] [2] [3].

Chemical reactor modeling is an essential tool for chemical engineering. From the context of process design, scale-up, or optimization, accurate models are invaluable to minimize the time and cost associated with these functions. The relative accuracy of the model, however, is dependent on the needs of the designer; not every model must encompass all known physical phenomena. There is always an observed tradeoff between realistic prediction and computational cost. Ultra-high-fidelity modeling, such as computational flow dynamics (CFD), can describe the development of complex flow fields in time by simultaneously solving three-dimensional mass and momentum balances. To achieve adequate resolution, the discretized

numerical solution requires protracted computation time to simulate a relatively minute time interval. As the scale of the reactor increases, the already excessive computational cost becomes prohibitively high for any practical use [1]. This issue is naturally compounded when additional complexity is introduced to the simulation, such as concentration step changes, localized substrate or cell culture monitoring, or reaction kinetics.

The back-of-the-envelope approach to bioreactor design involves coupling elementary ideal reactor models with kinetic expressions. Due to the complex nature of mixing that leads to concentration or temperature gradients and the potential for changes to bulk fluid properties as a reaction batch progresses, ideal models do not reflect real-world data. These models assume homogeneity, which does not address a chief concern for the effective operation of bioreactors. Proper mixing is essential for maintaining the specific conditions conducive to the life of cellular cultures in the process. Reaction parameters, such as temperature, concentration, and pH gradients, must be understood across a wide range of both temporal and spatial scales to ensure that the bioreactor is optimally designed. Additionally, a predictive mechanism for mixing effects due to intentional step changes (such as acid addition) or process upsets is desirable

Tracer tests for resident distribution time (RDT) in flow reactors provide insight into the actual flow distribution and mixing, and the ideal reactor models can be augmented by accounting for these tests. One example of these techniques is the tanks in series model, in which several uniform continuous stirred tank reactors (CSTRs) are placed in series to model the RTD obtained from a tracer test [4]. However, while this technique does refine the design and operational assessment of bioreactors, it cannot dynamically predict a response to a step change in a process parameter. The models developed from the tracer tests are limited in that they are

specific to the vessel for which the test was conducted, there is inherent uncertainty in the measurement, and their applications are typically restricted to flow reactors.

Compartment models (CM) of chemical reactors have the potential to offer higher fidelity than idealized models while offsetting the computational cost associated with CFD models by combining local and systemic approaches to modeling the chemical process [5]. In contrast to a CFD simulation, a compartment model can be used to quickly generate predictive information in real-time. This makes the compartment model approach ideal for simulating step changes, process control, decision-making, and process scale-up and optimization. A compartment model seeks to break a system into several zones or compartments that can be treated as ideal systems [5] [6]. This is not dissimilar to the tanks-in-series model discussed above except that compartments are generated with more inherent flexibility than that of the tanks in series approach. For model creation, the following general approach is taken by several authors [6] [7] [8]. First, flow information for a given vessel is parsed to generate idealized volume segments. Next, primary mixing data must be generated, and the reactor geometry must be specified. The reactor volume is then partitioned into smaller compartments or zones based on the generated mixing data. Each of these compartments is considered to be perfectly mixed. Volumetric flowrates (referred to as exchange flows) into and out of each compartment and adjacent compartments must be defined to account for circulation throughout the tank. From here, governing equations, typically in the form of ordinary differential equations (ODEs) for properties of interest, are developed based on mass and energy balances for each compartment.

As part of an ongoing project, creating a computational version, or “digital twin,” of a bench-scale bioreactor in the Chemical Engineering Department at Kansas State University is desired. The goal of a digital twin is to provide high-accuracy outputs in real-time. The power

of this is realized for obtaining information that cannot be measured experimentally and as a screening tool to aid in real-world experimental design. A CFD model has been developed for this vessel. However, this approach thus far is computationally expensive and eliminates the ability to generate information in real-time. Furthermore, to generate only 30 seconds of simulation, the solver requires time on the order of hours to obtain a solution. **This project aims to use the flow field data generated by the CFD model to develop a compartmental model that can then be used to approximate mixing times or parameter gradients in real-time.**

CHAPTER 1 - Sampled Literature

The core design choice behind the compartment model is the method by which compartments are generated. Broadly, model construction involves consideration for the total number of compartments and the connections between these compartments. Additionally, the volume of each compartment and flowrate between each compartment must be addressed. Various methods are employed to both obtain primary flow data and define compartments [5]. The two major methods for obtaining mixing information are data collection from an experimental apparatus [9] [10] or computational flow dynamics (CFD) simulation of a representative mixing regime [6] [7] [8] [11]. The compartment generation procedure is typically independent of the method by which flow information is obtained and can be either automated [10] [11] or manual [7] [8] [9], with advantages and disadvantages for each.

1.1 – Experimental-Based Compartment Models

Flow data is paramount to the compartmentalization of the agitated vessel. Empirical determination of the flow distribution is a more direct method than CFD simulation and allows for model validation to be inherent to the model development process. However, relying on instrumentation and manual measurement techniques to process data can increase the likelihood of errors.

Early development of compartment models often relied on designer judgment based on vessel geometry and experimentally determined flow velocity data. Tracer injection, impeller pumping calculations, flow-following devices, and a radio pill are all means of experimentally determining flow characteristics in an agitated vessel [9] [10] [12] [13]. The use of experimental data to generate a simplified flow/mixing model was first applied to bioreactors in order to

predict the oxygen consumption rate [14]. The developed model used five compartments, defined based on reactor geometry [14].

Another early example of an empirical compartmentalization approach was applied to a 30 m^3 fermenter [9]. Flow fields were developed using pulse-response experiments. A fluorescent tracer was injected into the test reactor at a known velocity and location. The compartments were determined based on the reactor geometry and circulation flows were calculated from the mixing data [9]. Expanding to the two-phase flow regime, Alvare et al. developed a compartmental type model for a trayed bubble column reactor in which a tracer was used to define the reactor as a series of CSTRs with back mixing [15].

More recently, the use of flow-following devices for flow characterization has been successfully applied to developing an empirical compartment model [10]. Bisgaard et al. developed a compartment model based on experimentally-obtained flow data. Flow-following devices were used to measure pressure at various locations throughout the reactor. These data were used to derive axial velocities along the height of the reactor and thus calculate the volumetric flowrate for specific cross-sections. Automated compartmentalization was then conducted to define compartment sizes and exchange flowrates. Only compartments along the vertical axis were generated based on the volumetric flowrate in the axial direction [10]. This implies that perfect radial mixing is assumed with this zoning technique and that mass transfer within the vessel is dominated by vertical movement.

To determine the compartment size, a parameter describing the local residence time was set equal to the compartment volume divided by the volumetric flowrate. The number of compartments was initialized arbitrarily with constant volume and could be increased or decreased based on comparing the calculated residence time for the compartment size and the

defined critical residence time. A reasonable prediction for mixing time was obtained using this method, with errors chiefly attributed to measurement limitations associated with the flow following sensors, particularly near the impellers where Stoke's number is much greater than the recommended value for the suitable use of flow tracers. The CM was analyzed through the lens of a CFD model as well. Exchange flowrates were calculated from the CFD simulation and compared to the experimentally determined flowrates. The axial flowrates from the manual and CFD data generation showed reasonable agreement, indicating that the flow-following devices could accurately measure the reactor's flow field. Finally, the experimentally determined mixing times for specific power inputs (in and of itself, a function of the impeller speed) were compared to the mixing times (defined as the time required to achieve 95% homogeneity) obtained from the compartment model. The comparison between the CM and the CFD predicted mixing times indicated that the threshold residence time of 0.95 seconds was appropriate for this application. It was postulated that this value for the threshold residence time might be more generally applicable [10].

There are inherent advantages to the manual data collection approach. Unlike CFD-based compartment models, model validation is not needed before proceeding with the development of the compartment model. In addition, these methods are versatile enough to be applied to multiphase, viscous, or reacting systems; CFD analysis is currently too computationally expensive to handle these more complex systems. Empirical methods are also relatively simple to implement, allowing for a good amount of agility for adapting to different reactor configurations and geometries. This is particularly advantageous for process control of a manufacturing process, where predictive modeling techniques may be needed to be applied to different existing vessels operating with similar conditions.

The advantages are somewhat offset by the inherent uncertainty in the measurement technique and difficulty with exchange flowrate calculations, such as the case of flow following devices near the impeller regions where velocity prediction has a significant error [10]. The source of the error can be related to the large Stokes number near the impeller regions. In much larger reactors, the Stokes number is smaller near the impellers [10]. As a result, the flow following devices may be more appropriately utilized for large-scale vessels already in operation.

While the empirical compartment models show a reliable fit to real-world conditions [10] [9], the major drawbacks include the need to have the vessel available for experimentation and the reliance upon the model designer's experience and judgment. The far more common approach to generating flow properties is utilizing computational flow dynamics to generate flow information, followed by compartment model development and model validation.

1.2 – CFD-Based Compartment Models

Although the development of the CFD model is not the focus of this report, the compartment model's generation relies on the developed CFD model. As a result, it is appropriate to provide a brief overview of computational flow dynamics and the application thus far toward stirred stank vessels.

CFD models numerically integrate flow equations to simulate fluid systems. Model inputs include a rigorous accounting of the vessel geometry and fluid properties. The fluid domains and problem boundary conditions must also be rigorously defined. For an agitated vessel, this includes separate domains for the fluid, the rotating planes, vessel walls, and the surface of the fluid. The fluid flow equations are then solved across a mesh of computational

nodes that digitally represents the physical vessel. Software, such as COMSOL [16] or FLUENT [17], is used to aid in model development and the finite element simultaneous solution of the Navier-Stokes and continuity equations, respectively presented as Equations 1.1 and 1.2:

$$\boldsymbol{\rho\left(\frac{\partial u}{\partial t}+u\cdot\nabla u\right)=-\nabla p+\nabla\cdot\left(\mu(\nabla u+(\nabla u)^{T})-\frac{2}{3}\mu(\nabla\cdot u)I\right)+F} \quad \textbf{(1.1)}$$

$$\boldsymbol{\frac{\partial p}{\partial t}+\nabla\cdot(\rho u)=0} \quad \textbf{(1.2)}$$

In Equations 1.1 and 1.2, u represents fluid velocity in meters per second, p is the pressure in pascals, ρ is the density in kilograms per cubic meter, and μ is the viscosity in pascal-seconds. Equation 1 accounts for the conservation of momentum by rigorously defining forces due to pressure, viscosity, inertia (I), and external forces (F). The continuity equation, Equation 2, accounts for the conservation of mass. The core working principle of computational flow dynamics is the simultaneous solution of Equations 1 and 2 for a given geometrical mesh, boundary conditions, and initial conditions.

To demonstrate the capability of CFD, Buss et al. [16] simulated a stirred vessel bioreactor. The model allowed the team to investigate double-pitched blades and Rushton-type impellers. Because changing a major piece of equipment such as an impeller is a nontrivial task in an industrial environment, it is helpful to have a predictive model to investigate vessel changes before commercial implementation. A range of impeller speeds was used to generate velocity fields and shear rates across the vessel's internal flow field. Using these data, the performance of the two different impeller designs was compared for the same power consumption and agitation rate. However, the simulation data was not validated using experimental techniques. As a result, neither dataset alone can be asserted to yield a reliable prediction for real flow properties. The generated model can, however, quantitatively compare the magnitude of difference in

performance between the different designs. Additional work for modeling bioreactors using CFD was performed by Shu et al. [17], in which CFD was combined with a standardized quality control method to optimize an aerobic fermenter. The CFD model was validated by using gas holdup times based on agitation speed and gas flowrate. The simulation data was regressed with the experimental data, with an R^2 value of 0.95, indicating reasonable agreement with the experimental measurements [17]. Once validated, an optimal configuration of process variables was developed. By performing an array of computations, the developed process control scheme can be directly implemented at scale for testing, eliminating the need for rigorous and expensive control strategy experimentation.

As evidenced by the previous two examples, computational flow dynamics is an excellent tool for determining flow characteristics within vessels for a constant set of fluid properties. However, adding multiple time and length scales, effectively creating sub-sets of algebraic differential equations for every computation node, exponentially increases the computational time. Current computing technology cannot solve these complex and evolving solutions using the rigorous finite element approach for a fine mesh. Compartment modeling allows for a CFD model, or series of CFD models, to be developed for constant bulk fluid property sets. These solutions can then inform the development of a generalized model that can be solved quickly and is flexible enough to incorporate the tracking of any number of variables, such as chemical reaction kinetics, temperature distribution, substrate concentration gradients, or mixing time. A cursory examination of a CFD solution reveals inherent patterns within a vessel's flow field. Chiefly, there are zones of low or high velocity. These zones have been differentiated via various means for generalized stirred tank reactors [18] [19] and model development using CFD to obtain the flow field data for use in compartmentalization has dominated recent methods for

modeling bioreactors. The chief variety among the developed models stems from compartment generation and application [7] [8] [11] [20] [21] [22] [23] [24]. The purely computational nature of the CFD-CM approach imposes the need for model validation with mixing time being the typical parameter of choice [10] [21] [24].

The predictive ability for bioreactor performance in industrial manufacturing processes is essential for design and performance rating. Early work for a CFD-coupled compartment model was applied to xanthan gum production with a generic reactor geometry [20] [25] [26]. This work first utilized the concept of automatically defining geometric reactor zones based on a single parameter threshold. Then the compartments within the reactor were developed based on the predicted viscosity variation due to induced shear [20] [26]. This automated zoning strategy was an attempt to minimize the number of required compartments and remove the potential source of error associated with using human judgment to subdivide the reactor. The key learning from this early work in CFD-CM automated zoning is that the parameter of interest for developing an algorithm depends on the studied system.

In contrast, a purely manual method of defining compartments from CFD output was explored for the general case of mixing in a stirred tank bioreactor [27]. The initialization of compartment volumes is conducted through organizing CFD cells into equal-volume partitions. Flowrates between compartments are calculated directly from CFD data and are differentiated between a mean flow rate and a turbulent flowrate, the latter being computed from the turbulence kinetic energy predicted by the CFD model. Each zone is connected to two adjacent compartments via the mean flowrates and turbulent flowrates. This manual method of compartmentalization was found to be advantageous due to the ease of implementation. The major drawback to this method of compartmentalization is the necessity to generate a very large

number of compartments. The best prediction was observed when the discrete number of compartments generated from the CFD output was greater than 13,000 [27] as opposed to the maximum of 25 reported in an automated zoning method [20]. While mixing time and concentration distribution throughout the axial position in the reactor is well-represented between the CFD model and the compartment model [27], this increased resolution and the relatively simple implementation are somewhat offset by significantly greater computational cost (13,000 ODE sets versus 25 ODE sets). Incorporating additional process considerations, such as reaction kinetics, will require the addition of at least 13,000 ODEs per parameter. A similar approach of compartment generation has been recently applied in conjunction with intracellular models to examine an industrial penicillin bioreactor [28]. It was demonstrated that good model agreement could be obtained from a CFD-CM that runs on the order of minutes. By comparison, incorporation of the Euler-Lagrange approach with CFD for tracking performance based on intracellular responses requires weeks to solve [28].

Beyond general cases, CFD-CM has been applied to a variety of reactor sizes for various modeling goals using diverse compartmentalization techniques [7] [8] [20] [21] [22] [23] [24] [29] [30]. At a base level, CFD-CMs are developed to account for mixing effects [29] [30]. Krychowska et al. used a CFD solution to fit mathematical modeling parameters to a geometrically-developed compartment model of a commercially available pilot reactor. Compartment volumes were calculated based on geometrically similar areas, exchange flows were determined directly from the CFD simulation, and parameters were fitted to the overall mass balance until the CFD-CM was able to mimic the CFD and RTD results [29]. A multiphase loop reactor is considered by Weber et al, incorporating mixing information obtained from CFD

to define the continuous phase and Monte-Carlo simulation to account for the dispersed phase [30].

Biokinetic mechanisms were incorporated into a CFD-CM approach to a pilot gas/liquid reactor by Moullec et al. [23]. The reactor of interest is utilized for aerobic wastewater treatment. Gas is injected into the bottom of the flow length, and wastewater water flows through a channel. The authors note that hydrodynamics affect the pollution removal efficiency with a biological kinetic mechanism that is represented well by Monod kinetics with greater than zero reaction order [23]. The connotation here is that using a compartment or CFD type of model rather than a system of idealized models will provide a more accurate representation of the physical process because these models account for the hydrodynamics of the system, whereas a simple kinetic model does not.

Additionally, if a model is used to design or verify a waste treatment facility, then it must not overpredict performance. Compartments were generated manually to account for the complexity of the two-phase flow and the variable channel geometry [23] based on knowledge of reactor geometry and analysis of CFD results. The length of the channel was split into zones of equal sizes. Each zone contained 4 compartments. The compartments were designated based on the gas fraction, the liquid velocity field, and the liquid turbulence characteristics. Flowrates between two adjacent compartments were calculated directly from the CFD simulation using velocity and compartment flow area to determine the volumetric flowrate [23]. The main purpose of CFD in a model such as this is to describe the internal flow field, then use this description to qualitatively define zones and quantitatively define exchange flowrates between these zones. While designer judgment is used to set up compartments, the approach is still somewhat automated by using directly calculated exchange flowrates.

Norregaard et al. [24] referred to a “hypothesis-based” compartment model, where the strategic placement of division leads to a systematic development of reactor compartments. The authors outline a 5-step process for developing the model from CFD output. First, vertical lines are imagined in the mixed tank, and the radial velocity is determined along each line from top to bottom of the reactor [24]. These divisions are created arbitrarily and placed so the modeler can find a balance between computational expense and the total number of compartments. At certain points along the axial division lines, the radial velocity will change from positive to negative values, denoting a flow direction change. The point at which the flow changes direction is defined as the axial division and is considered to have a net radial velocity of zero [24]. These zero points then serve as markers for the placement of axial divisions of the reactor, where the process is repeated for axial velocity [24]. Finally, the circumferential division at the baffles is determined, and the flows between the compartments can be identified [24]. This method directly generates compartments based on velocity via this method. A major strength of this method is the ability to generate compartments based on a single parameter and, more importantly, without the need to incorporate system-specific variables. However, many compartments are generated, which drives up the computational cost. The authors state that kinetics and mass transfer phenomena can be incorporated into the framework, but this is not explored in the paper [24]. Although the zero velocity points are used to define compartments, this approach is still only semi-automatic, as good placement of the initial divisions will determine model performance.

It should also be noted for the previous two approaches [23] [24] that if a CFD-CM approach is used for a reacting system, the system must retain nearly constant bulk fluid properties, such as density and viscosity. The other option is to predict the bulk property changes

based on the extent of reaction, then to generate multiple CFD models using a range of fluid properties to simulate the flow characteristics throughout a reaction. The local velocity points will change with changes to bulk fluid properties, assuming a constant mixing power input. Compartmentalization and quantification of exchange flows can be conducted for each of the CFD models. For the application of the compartment model, the kinetic model is used to predict fluid property changes in real time. As the fluid properties change, the exchange flowrates or compartment volumes must change to match the CFD data for the changes to the flow characteristics. It may also be possible to affix compartment sizes based on a set of initial conditions and define exchange flow as a function of reaction conversion based on the CFD velocity outputs, thus removing the need for compartmentalization for every CFD model produced.

Spann et al. studied industrial-scale lactic acid bacterial cultivation [21]. This modeling approach took a more structured yet manual path to develop a compartment model for a 700-liter stirred tank bioreactor. A CFD model was first generated and verified using pH tracer measurements. Next, the compartments were generated by analyzing the flow fields in the bioreactor. At every 1 centimeter of height in the CFD model, the axial velocities and node areas were obtained, and the average of up and down flows was calculated. By separating the positive average axial velocities, local minima were observed that correlated to boundaries between well-mixed zones in the reactor. These are further reinforced by local maxima of downward velocities at the same location. The average velocity in the upward and downward direction is used in conjunction with the flow area to determine the exchange flowrates between the compartments [21]. This is not dissimilar to the method utilized by Bisgaard [10], except that compartment definition was retained in both the axial and radial directions. With each compartment's volume

and exchange flow, biokinetic and pH models were implemented separately into each contiguous compartment [21]. The compartment model effectively predicted pH and concentration gradients throughout the reaction volume. The intended application of this model is as a soft sensor for real-time process monitoring and risk analysis [21]. The rapid computation time, coupled with the reasonable predictive abilities of the model, makes this a viable method for implementation across multiple reactor geometries and anaerobic bioprocesses.

The CFD-CM approach has been applied to manufacturing operations and wastewater systems with less strictly controlled reaction parameters [7]. The CFD compartment modeling approach was coupled with a kinetic model for anaerobic digestion used in wastewater sludge management [7]. This study took a manual approach to compartmentalization, generating compartments individually based on the velocity distribution in the vessel. An inherent disadvantage to manual zoning is that the robustness of the generated compartments is often dependent on the researcher's experience and expertise. Manual compartmentalization, mainly based on CFD modeling, is more challenging to apply to reactors of different geometries and sizes. However, it does allow for more freedom and ease of generating the compartments once the geometry is established and the CFD data is available. The procedure involves partitioning the reactor into four distinct zones: a high-velocity zone, a medium-velocity zone, a low-velocity zone, and a stagnant zone [7]. These zones were used to further subdivide the reactor into eight distinct compartments (modeled as ideal CSTRs) based on the residence time [7]. While the model's results were not compared to real-world validation data, the point was made to show that when flow considerations are taken into account, treating the anaerobic digestor as an ideal CSTR is inappropriate. Intriguing information is also obtained about the role of individual

compartments in overall reactor performance. This information can aid in making design choices for commercial vessels, such as impeller type, baffle placement, or mixing speed.

Many bioprocesses are aerobic, and the dissolved oxygen concentration plays a significant role in the local kinetics of the system. Oxygen can be treated as an additional substrate in the kinetic modeling of bioprocesses [31]. Incorporating dissolved oxygen into bioprocess modeling provides additional difficulty due to the relatively rapid kinetics, increasing model stiffness [32]. As a result, the already great computational demand for ultra-high-fidelity modeling is increased, and small changes in the CFD input may yield inconsistent results [32]. In pilot and bench scale process development, bubbling air results in a relatively uniform distribution of bubbles and dissolved oxygen; the fluid flow field tends to be homogenous. As a result, the gas and liquid phases do not have to be accounted for independently. In larger vessels where the gas holdup in the liquid is greater, the distribution of air bubbles loses uniformity, and the flow fields of both phases can act independently. An accurate model must consider the gas and liquid phases independently [22]. Modeling a heterogenous mixture with CFD greatly increases the computational cost. To overcome this challenge, Nauha et al. [22] applied the compartment modeling approach to an industrial-scale bioreactor with a large gas flow. The developed model was a combined CFD-compartment model with a semi-manual zoning technique. The compartmentalization was performed directly within the CFD software using a user-defined function. A time-average solution was first generated, then compartments were created in similar-flow regions. To mitigate errors due to improper compartmentalization, the researchers generated many compartments (over 100). The bubble size distribution for the sparged airflow within each compartment was monitored using a population balance equation. Breakage and coalescence were modeled using empirically-fitted equations [33] [34] [35] [36].

This particular study aimed to compare the results obtained with the compartment model with the results obtained with the CFD model [22]. However, large-scale experimental data was not available for model verification. The CFD results did show good agreement with the compartment model and indicated that it might be an effective tool for scale-up from the bench-top reactor once verified experimentally. By contrast, Gimbun et al. also developed a CFD-CM for a gas-liquid stirred tank, coupling the compartmentalization strategy with a population balance model. However, compartments are generated manually based on reactor geometry, with volumes and exchange flowrates adjusted with parameters to force a good fit [37]. Coupling the population balance model with a CFD-CM certainly shows promise for rigorous accounting for the dissolved oxygen profile within a reactor. This is particularly important for determining the sparging rate and scale-up effects for aerobic bioprocesses.

The population balance model coupled with the CFD-CM [22] [37], similar to coupling a CFD-CM with a kinetic model [7] [20] [21] [23] [25] [26], is inherently more computationally expensive than those examining only mixing effects. For example, in the case of the population balance model, a large number of compartments may be needed to minimize error [22]. Adding additional elements to the CM such as kinetic modeling or rigorous substrate monitoring will further increase the computational load. As computation time increases, the versatility of the model decreases. This type of model would be useful for scale-up, but probably not for real-time process control or monitoring. As an alternative to a single, all-encompassing CM, it might be possible to develop a series of CMs. To illustrate this, consider the output of an oxygen concentration CM serving as the input for a CM that calculates cellular growth. This allows for the models to be compiled separately or step-wise, decreasing the short-term computational load

and allowing the designer to pick and choose the degree of fidelity. As a result, both process control and scale-up applications can be realized.

The CFD-CM approach has also been applied to variable volume processes, such as a fed-batch bioreactor [8]. Nadal-Rey et al. examined a fed-batch fermentation reactor, accounting for fluid dynamics, volume changes, and fermentation kinetics. The process involved generating CFD models for the same reactor geometry at different volumes. The output of each CFD was then automatically compartmentalized using radial and axial velocities, following the same compartmentalization method reported by Tajsoleiman et al. [11]. When the dynamic compartment simulation was performed, the model discretized total volume increments in the reactor and assumed the compartment configuration closest to the CFD volume used. As a result, each compartment was evaluated along a predetermined volume range, with periodic remapping of the compartments [8]. The compartment model showed reasonable agreement with the CFD models when tied to the kinetic model, with a significantly reduced computation time. 90 seconds of simulation required about 30 days with 24 CPU cores for CFD, while the same simulation time required 2 seconds with a single core for the compartment model. This case is significant as it illustrates the potential for a dynamic response in compartmentalization. Reactor compartments can be initially defined, then either grow or have exchange flows change based on operating conditions and governing functions.

The presented literature for CFD-CMs demonstrates that, in general, local velocity or another discrete parameter calculated from CFD is used to differentiate different zones or compartments within the reactor. Both automated and manual methods diverge based on the modeling goal or researcher preference. Applications of compartment models universally involve predictive simulations for bulk parameters. At the cost of fidelity, computational speed is

reduced from the order of days (CFD) to the order of seconds. The above cases demonstrate that while the general methodology for compartment model development for bioreactors is well-established, there is no agreed-upon procedure for reactor zoning. As can be observed from the available literature, the employed zoning methods are, for the most part, not repeated across different reactor geometries or conditions.

The current work seeks to examine an existing method for compartmentalization from experimentally-determined flow information [10] and adapt this zoning methodology for use with a CFD model developed by collaborators at Kansas State University. Although CFD was used as a comparison for this particular method, only predicted exchange flowrates were examined; the study was not expanded to compare CFD-generated concentration profiles or bulk mixing times [10]. A comparison of results for the model developed through this method and the CFD model with coupled momentum and mass balances will be examined for scenarios involving a concentration step change. For this baseline study, airflow is not considered. This investigation will qualitatively examine the efficacy of using a CFD-generated velocity distribution for the zoning method. The residence time threshold established by Bisgaard et al. will be tested to determine if it is appropriate for a different reactor geometry. Additionally, the bulk mixing time and axial concentration distribution for the generated compartment model will be compared to the CFD solution.

CHAPTER 2 - Methodology

This chapter describes how the compartmentalization approach previously outlined by Bisgaard et al. [10] is modified for use with CFD solutions. First, a CFD model is developed to simulate a real-world pilot-scale bioreactor. The z-direction velocity distribution calculated by the CFD simulation is then used to compartmentalize the reactor into idealized mixing zones. The efficacy of these mixing zones is then tested by simulating process step changes or pulse injections of acidic media.

2.1 Bioreactor Configuration

The bioreactor is a cylindrical agitated vessel equipped with pH and dissolved oxygen sensors, a centrally-located agitator, a heating/cooling coil, and an air injection port. The physical dimensions of the reactor are summarized in Table 2.1. An experimenter can control impeller speed, injection air flowrate, and temperature using a built-in controller.

Table 2.1. Geometrical details of the bench-Scale bioreactor at Kansas State

Vessel Height	32.5 cm
Vessel Diameter	18 cm
Impeller Diameter	1.19 cm
Blade Width	1.55 cm
Blade Height	1.8 cm
Blade Support Diameter	3.1 cm
Blade Support Thickness	1.8 cm
Relative Height of Blade Set 1 from Bottom	5.5 cm
Relative Height of Blade Set 2 from Bottom	14.5 cm
Air Injection Height (centered)	3.5 cm

Figure 2.1. A photograph of the bioreactor in operation with air injection and agitation

2.2 – CFD Simulation

The CFD simulation of the reactor specified in the previous section was created using COMSOL. As discussed in Chapter 2, CFD relies on the solution of simultaneous partial differential equations (PDEs), namely, the Navier-Stokes equations and the continuity equation

solve for the local velocity at each point in the reactor mesh. Therefore, a three-dimensional model was created that mimicked the geometry of the real-world apparatus (Figure 2.1 shows the actual reactor while Figure 2.2 shows the digital rendering), and a mesh was developed to solve the simultaneous PDEs (shown with Figure 2.3).

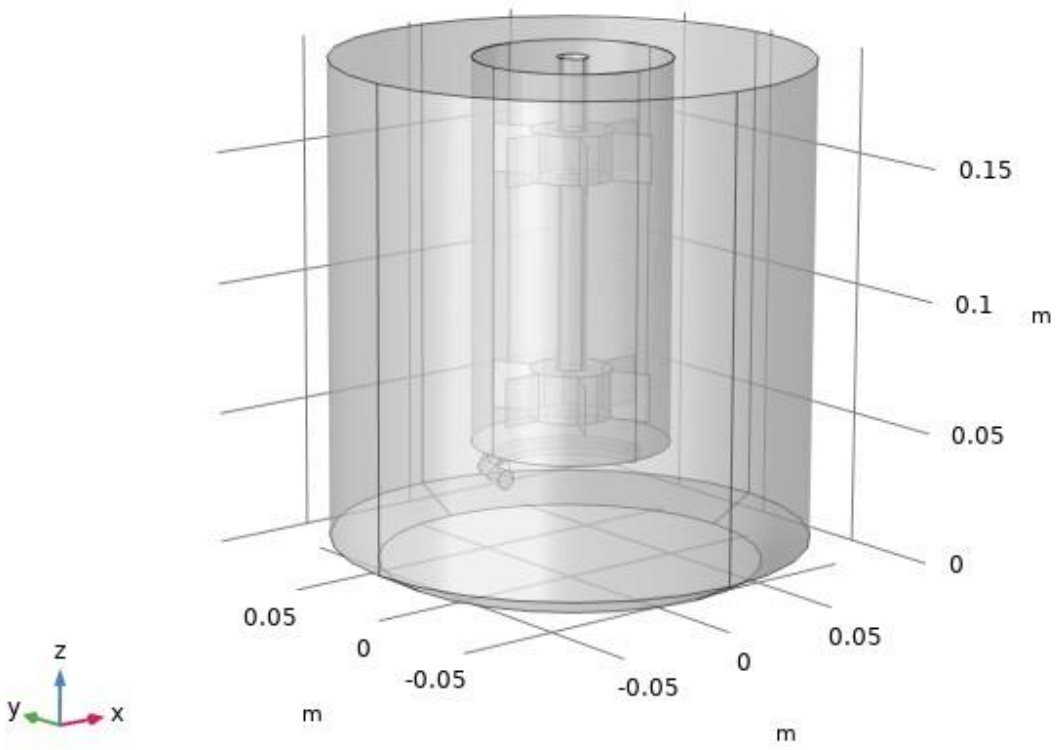

Figure 2.2. Digital rendering of the real-world reactor with an assumed fluid height, z, of 19 centimeters

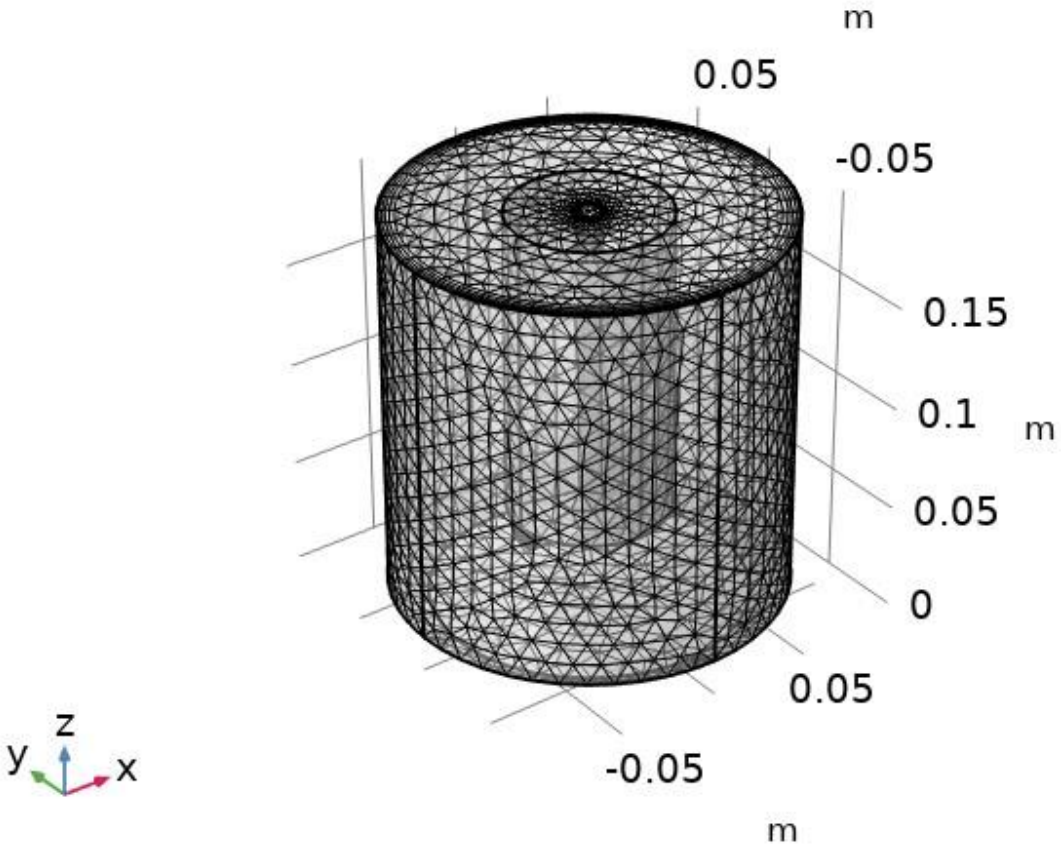

Figure 2.3. Solution mesh for solving PDEs associated with the velocity distribution. x,y, and z velocity is calculated discretely at each node.

To account for the two-phase effects of the injected airflow, the Navier-Stokes equation was modified to account for the volume fraction of the second phase. The gas phase was described using a volume fraction field, and the volume fraction of gas was calculated alongside velocity for each discrete node, as summarized in Equations 2.1 and 2.2:

$$\boldsymbol{\rho_{liq}\frac{\partial v_{liq}}{\partial t} + \rho_{liq}(v_{liq}\cdot\nabla)v_{liq} = \nabla\cdot[-pI + K] + \phi_{liq}\rho_{liq}g + F} \quad \textbf{(2.1)}$$

$$\boldsymbol{\frac{\partial \phi_{gas}\rho_{gas}}{\partial t} + \nabla\cdot(\phi_{gas}\rho_{gas}v_{gas}) = m_{gl}} \quad \textbf{(2.2)}$$

where ϕ_{gas} represents the average local volume fraction of air. To aid in the solution, homogenous flow was assumed, and the gas phase velocity was set equal to the velocity of the liquid phase. For smaller vessels such as this bench-scale apparatus, this assumption is valid [22] The solutions for the three-dimensional unsteady-state differential equations were solved using the finite element methods with a no-slip boundary condition at the reactor walls and fluid surface. A solution was sought for an impeller speed of 50 rotations per minute (rpm), the case of no airflow, and the case of 5 liters per minute airflow.

2.3 – Compartment Model Development

The velocity output from the CFD model was used to develop the compartment model. It was assumed that mixing effects due to the x and y velocity components were negligible compared to the axial velocity component. In other words, mixing effects were driven primarily through fluid movement in the z-direction, with radial fluid movement mostly homogeneous. The z-component velocity profile across the x,y plane was collected across the fluid height at each centimeter, as represented in Figure 2.4.

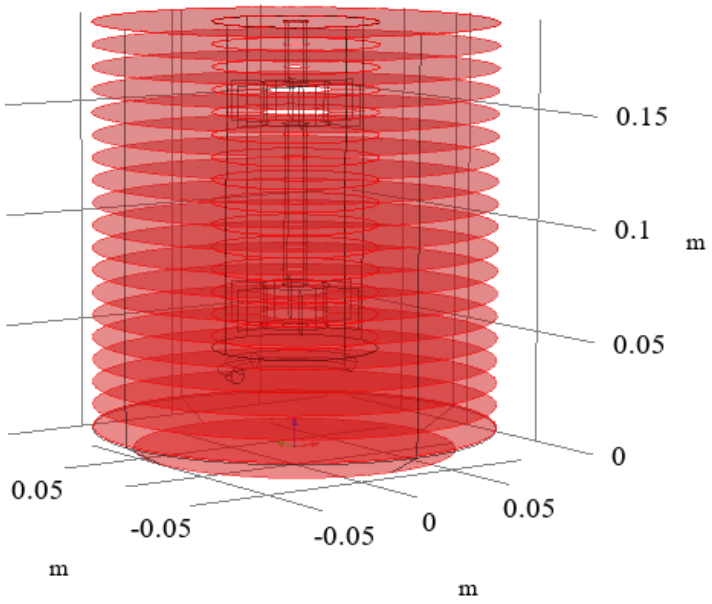

Figure 2.4. The axial velocity at each centimeter of reactor height was collected for all discrete nodes along the corresponding x,y plane, allowing positive and negative velocities to be processed independently.

Once the velocity information is organized, the volume and exchange flowrate across each compartment can be determined. The network of compartments is represented graphically in Figure 5.

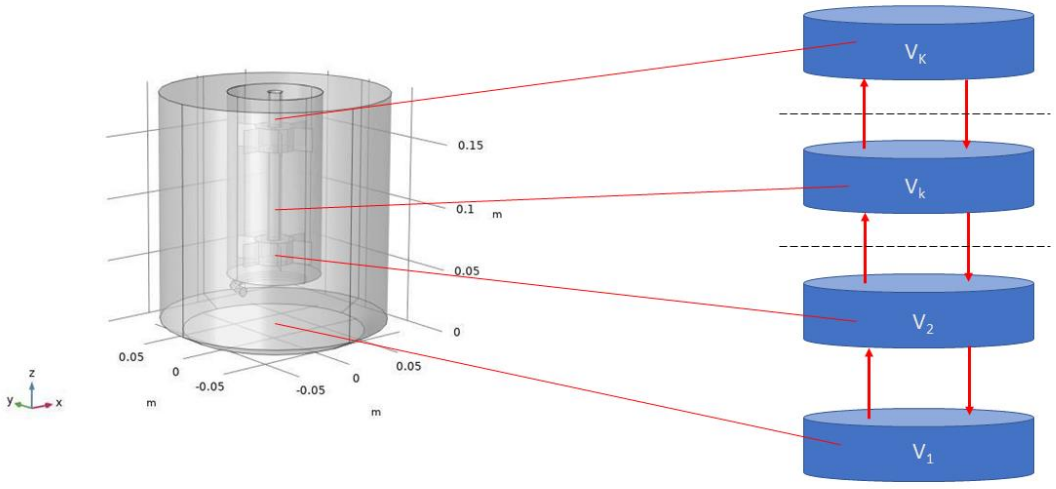

Figure 2.5 The physical reactor geometry is axially subdivided into cylinder-shaped compartments. Internal components are not considered for the baseline case. Each of these zones is considered well-mixed, and the flow field is represented by the flowrates into and out of each compartment.

2.3.1 – Compartment Generation

The average positive and negative axial velocities were calculated from the obtained velocity distributions for each centimeter of fluid height. The average positive and negative volumetric flowrate at each point is then calculated from the plane's average upward velocity, downward velocity, and surface area. As an initial modeling estimate, the volume occupied by the impeller and blades was ignored entirely to determine the average flowrates. For reference, this area accounts for approximately 1 cm^2 across the x,y plane vs. a total area of over 250 cm^2. So while the calculated volumetric flowrates and surface areas are not technically correct, the minor loss in fidelity was considered worth the computational relaxation. Later, the initial condition of a concentration step change was adjusted to account for the volume difference

between the CFD model and the compartment model. The average volumetric flowrate across each x,y plane is calculated from equations 2.3, 2.4, and 2.5, and the volumetric flowrate for a given internal compartment, k, is calculated from equation 2.6.

$$\boldsymbol{Q_{up} = v_{up} A_{plane}} \quad \textbf{(2.3)}$$

$$\boldsymbol{Q_{down} = v_{down} A_{plane}} \quad \textbf{(2.4)}$$

$$\boldsymbol{A_{plane} = \pi r^2} \quad \textbf{(2.5)}$$

$$\boldsymbol{Q_k = Q_{up} - Q_{down}} \quad \textbf{(2.6)}$$

Next, the compartments are initialized as 19 identical volumetric cylinders, each with a height of 1 centimeter. The average volumetric flowrate for the vertical compartment is used to calculate the residence time within the compartment, as denoted by equation 2.7:

$$\boldsymbol{\tau = \frac{Q_k}{V_k}} \quad \textbf{(2.7)}$$

where the residence time in a given compartment is denoted by τ and the volume for a given compartment is denoted by V_k. The volume is considered to be that of the cylinder generated by linking two of the planes for a given height, h:

$$\boldsymbol{V_k = \pi r^2 h} \quad \textbf{(2.8)}$$

Based on the procedure outlined by Bisgaard et al. [10], the initial compartments were then combined with a goal residence time of τ~1 second or less.

2.3.2 – Modeling a Concentration Step Change

Once the compartments and exchange flowrates were specified, the concentration distribution in the reactor was modeled. 1 mL of 98% sulfuric acid addition to the top of the

reactor was simulated for this step change. The initial condition was, therefore, the molarity of hydrogen ions at the top of the reactor, assuming perfect mixing in the top compartment. The change in concentration was then calculated for internal compartments (k), the uppermost compartment (K), and the bottom compartment (designated compartment 1) by using mass balances displayed using equations 2.9, 2.10, and 2.11:

$$\frac{dC_1}{dt} = \frac{1}{V1}(C_2Q_1 - C_1Q_1) \quad \textbf{(2.9)}$$

$$\frac{dC_k}{dt} = \frac{1}{V_k}(C_{k-1}Q_{k-1} + C_{k+1}Q_k - C_kQ_{k-1} - C_kQ_k), k = [2\ (K-1)] \quad \textbf{(2.10)}$$

$$\frac{dC_K}{dt} = \frac{1}{V_K}(C_{K-1}Q_{K-1} - C_KQ_{K-1}) \quad \textbf{(2.11)}$$

The simulation of acid addition allows for the direct calculation of the pH distribution using equation 2.12:

$$pH = -log_{10}[H^+] \quad \textbf{(2.12)}$$

This will allow for model validation using the existing bioreactor if there is interest. The simultaneous ordinary differential equations (ODEs) were solved using ODE45 built-in function in MATLAB R2021b. By tracking concentration rigorously, an estimated axial distribution can be observed for any point in time, t. Additionally, the total mixing time can be estimated from the convergence of the compartment concentrations. This step change was modeled as an initial condition for the top ½ cm of the reactor. It was assumed that a well-mixed concentration zone existed at this point to compare the mixing predicted by the CFD and the compartment model.

In addition to a step change with an initial concentration at time zero, a pulse injection to the top of the reactor was simulated as 1 mL per second of sulfuric acid for the first 10 seconds of the simulation. This was achieved by directly accounting for the addition of moles of H+ to the concentration balance for the top compartment CFD-CM model for the first 10 seconds.

After this, the injection was stopped while the simulation continued for another 60 seconds. This simulated injection was performed with the CFD model and the CFD-CM model for comparison. The injection pulse used with the CFD model is shown graphically in Figure 2.6

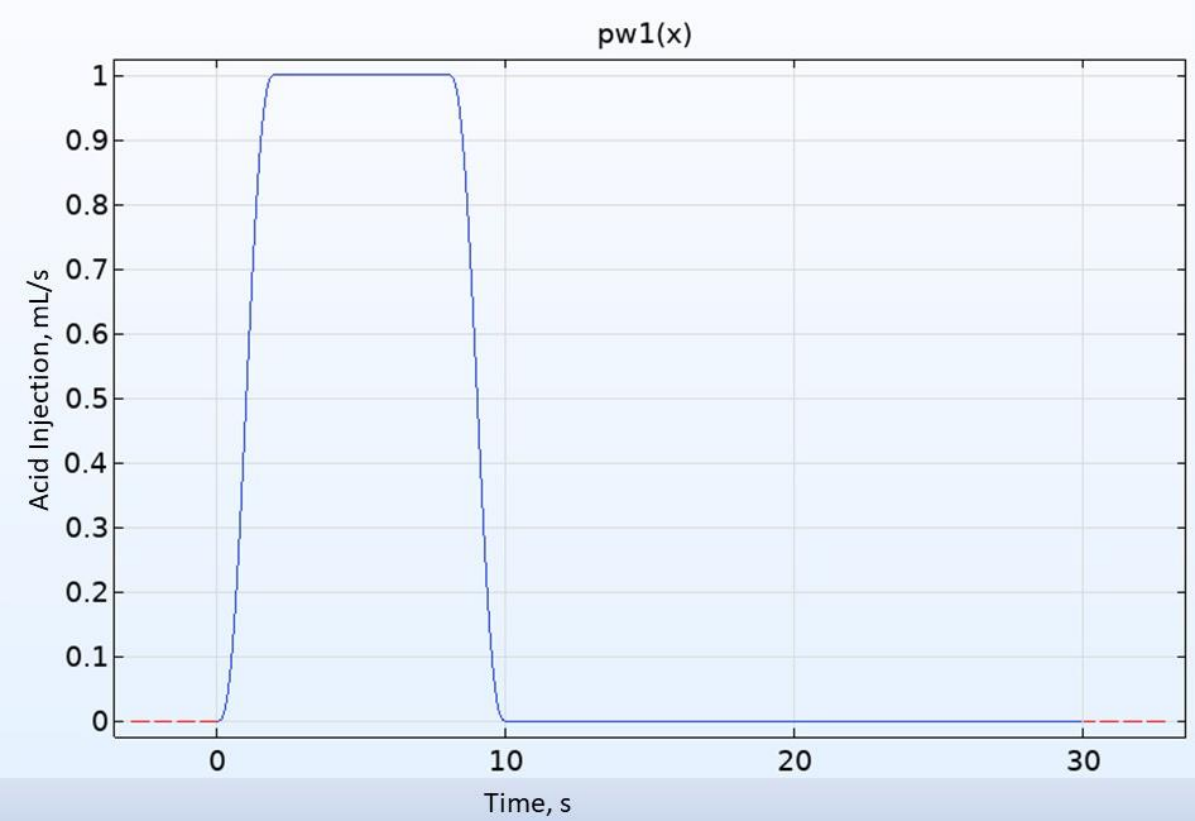

Figure 2.6. Acid injection flowrate as a function of time.

In order to simulate the acid injection using CFD, a time-dependent boundary was established in the form of a circular section at the liquid surface. This boundary represented an injection point. The diffusion coefficient was taken into account for the overall mass transfer modeling. The injection hole had an assumed radius of 2 millimeters, and the total pulse span was 10 seconds. Approximately 8-10mL of acid was injected with a velocity of 0.0796 m/s. As a result, the injections simulated between the CFD model and the CFD-CM model are not identical, but are reasonably similar, given the relative accuracy. This is fundamentally different

from the injection to the CFD-CM model, which calculates an updated and homogenized top compartment concentration based on a constant molar addition.

CHAPTER 3 - Results and Interpretation

3.1 Compartment Generation

The output files containing the axial velocities across the x,y plane for each centimeter resulted in an initial compartment number of 20. Due to the no-slip boundary condition at the liquid surface, de minimis velocities are calculated near Z = 19cm and Z = 0cm. The top compartment was split in half to avoid a gross overestimation of the mixing time, with a larger average velocity on the lower half. By averaging exchange flows and calculating residence time, the total compartments were reduced to 12, easing computational demand. The results of the compartmentalization are summarized in the following tables. Table 3.1 shows the initial compartmentalization with residence times and exchange flowrates, and Table 3.2 shows the compartmentalization after implementing the compartment reduction algorithm.

Table 3.1. Initial compartmentalization of CFD results.

Compartment	Z Range(cm)	Q (cm^3/s)	V (cm^3)	τ (s^{-1})
1	0-1	121	254	2.11
2	1 to 2	337	254	0.75
3	2 to 3	487	254	0.52
4	3 to 4	590	254	0.43
5	4 to 5	743	254	0.34
6	5 to 6	1063	254	0.24
7	6 to 7	1139	254	0.22
8	7 to 8	787	254	0.32
9	8 to 9	516	254	0.49
10	9 to 10	431	254	0.59
11	10 to 11	448	254	0.57
12	11 to 12	543	254	0.47
13	12 to 13	653	254	0.39
14	13 to 14	808	254	0.32
15	14 to 15	993	254	0.26
16	15 to 16	836	254	0.30
17	16 to 17	462	254	0.55
18	17 to 18	244	254	1.04
19	18 to 18.5	155	127	0.82
20	18.5 to 19	77	127	1.64

Table 3.2. Compartment volumes and residence time after implementation of the compartment minimization algorithm.

Compartment	Z Range (cm)	Q_k (cm^3/s)	Vk (cm^3)	τ (s^{-1})
1	0-1	121	254	2.11
2	1 to 2	337	254	0.75
3	02 to 4	538	509	0.95
4	4 to 7	941	763	0.81
5	7 to 9	787	509	0.65
6	9 to 10	431	254	0.59
7	10 to 12	497	509	1.02
8	12 to 15	823	763	0.93
9	15 to 17	668	509	0.76
10	17 to 18	244	254	1.04
11	18 to 18.5	155	127	0.82
12	18.5 to 19	77	127	1.64

3.2 – Concentration Step Change: 12 Compartments

The resultant pH distribution in the reactor from the simulated addition of 1mL of 98% sulfuric acid is displayed graphically for different mixing times in Figure 3.1.

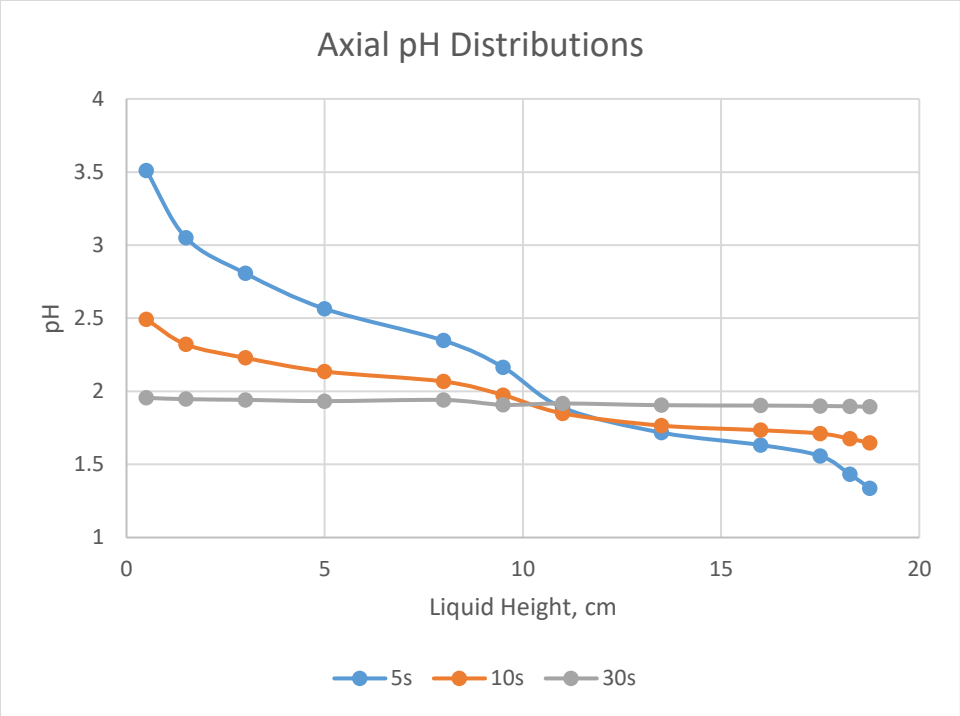

Figure 3.1. Axial pH distribution for different mixing times. Note that each data point represents a homogenous concentration volume within the vessel.

To illustrate the predicted mixing time, Figure 3.2 shows the pH as a function of mixing time at three different reactor heights.

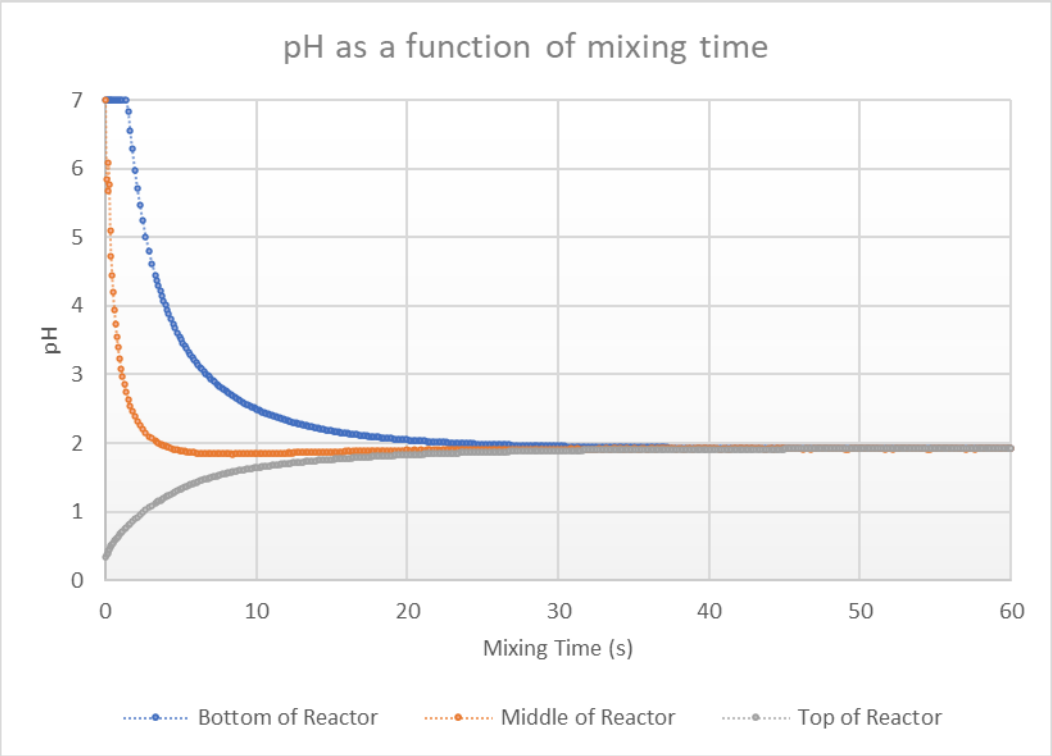

Figure 3.2. pH changes across a 60-second mixing range based on an initial concentration condition at the top 0.5 cm of the reactor

The pH of the reactor reaches a mostly converged distribution centered around 2.12 after 30 seconds of mixing. Therefore, the model predicts only an infinitesimal change in compartment pH after 30 seconds. However, if the simulation can proceed to approximately 120 seconds, the solution effectively converges to a final pH of 2.12. In contrast, the final theoretical pH of the bulk solution after an addition of 1mL of 98% sulfuric acid is predicted to be 2.14 based on a simple pH calculation for the volume of the vessel. Therefore, the mixing model predicts the converged pH with an error of 0.9%.

However, when the CFD-CM is compared to the axial pH distribution, it becomes clear that neglecting the internal volume components created a significant disparity between the two models, as demonstrated by Figure 9.

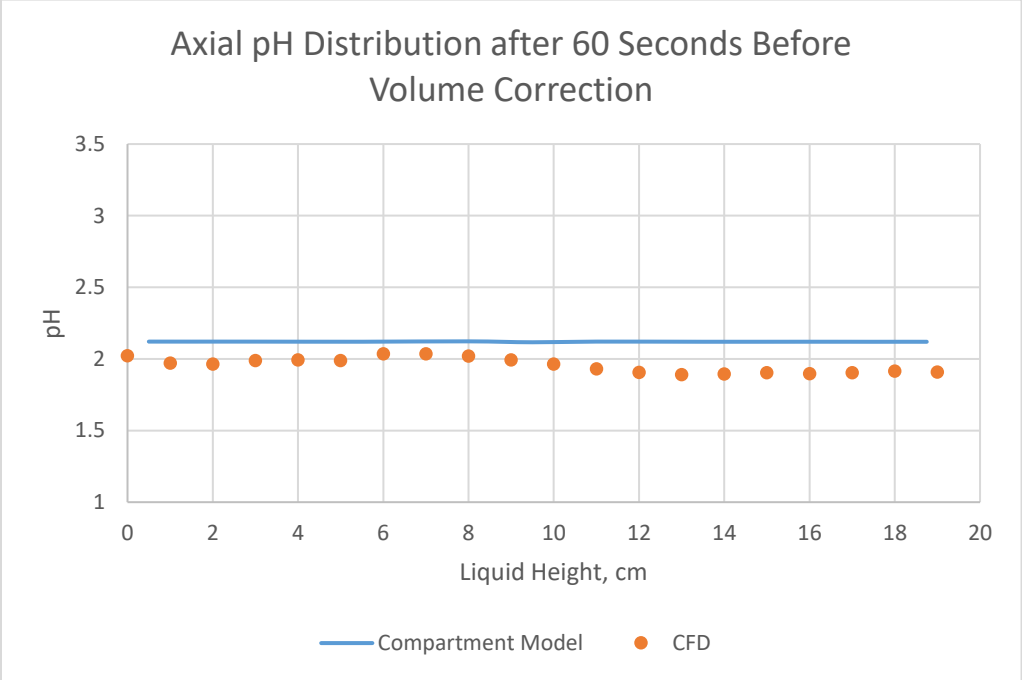

Figure 3.3. Comparison of CFD pH and CFD-CM pH after 60 seconds of mixing

To account for the disparate internal volumes between the two reactors, the initial acid concentration at the top of the reactor model was adjusted to match the predicted molar addition of the CFD model. More specifically, rather than adjust the internal volume of the compartments, the dose of acid was increased so that the concentration matched. When the volume was compensated for, the models showed decent agreement, displayed graphically with Figure 3.4:

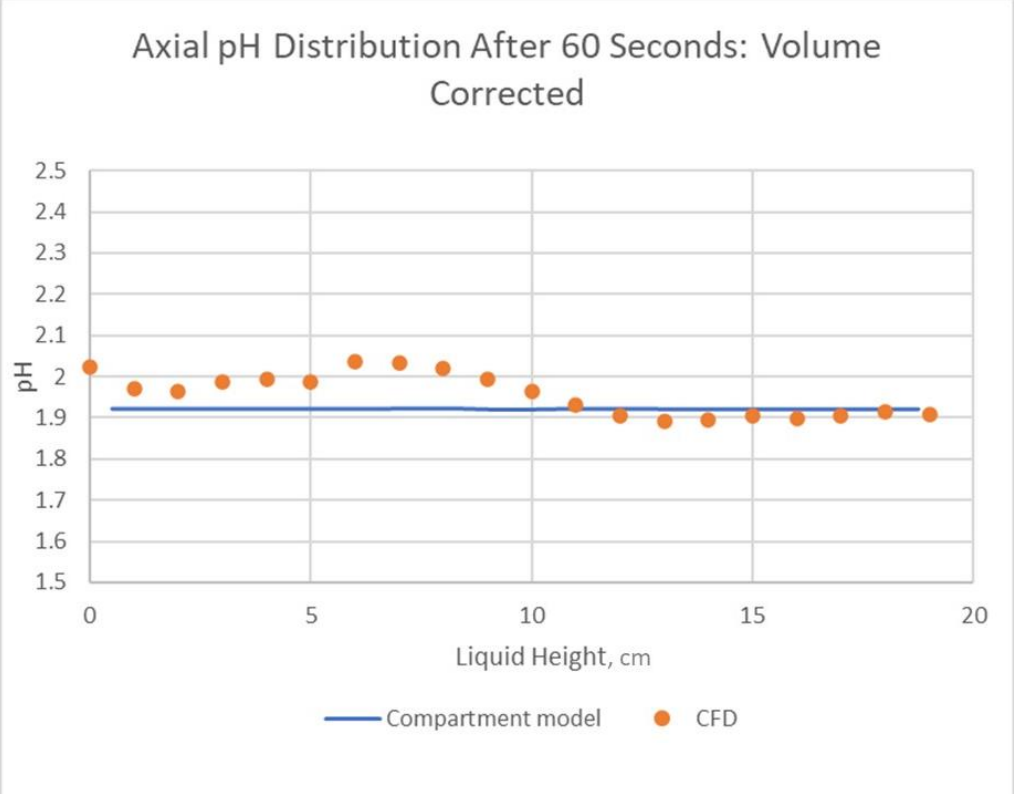

Figure 3.4. After volume adjustment, the compartment and CFD models show agreement after 60 seconds of mixing.

The comparison along the axial positions for both models is given in Table 3.3:

Table 3.3. Comparison of simulated reactor pH at different heights after 60 seconds of mixing.

Z (cm)	CFD-CM pH	CFD pH	%difference
0.5	1.92	2.00	3.77%
1.5	1.92	1.97	2.36%
3	1.92	1.99	3.35%
5.5	1.92	2.01	4.57%
8	1.92	2.02	4.85%
9.5	1.92	2.01	4.46%
11	1.92	1.93	0.46%
13.5	1.92	1.89	1.52%
16	1.92	1.90	1.21%
17.5	1.92	1.91	0.61%
18.25	1.92	1.91	0.43%
18.75	1.92	1.91	0.56%

The error calculated between the two models is less than 5% along all axial positions. It is to be expected that the CFD model produces a higher resolution axial pH distribution than the compartment model, and so other considerations may account for the slight pH variation such as radial flow effects. All values in the pH distribution predicted by the CFD model are within a 95% confidence interval for the sample set. It can be concluded, therefore, that the models are in reasonable agreement for the estimation of total mixing time.

3.3 – Concentration Step Change: 20 Compartments

To test the agreement between the CFD simulation and the compartment model approach, the residence time threshold was tightened from ~1 second to as short as possible given the available data to generate 20 axial compartments. The axial pH distribution at different time intervals and the pH evolution at different reactor heights for 60 seconds of mixing time are given in Figure 3.5 and Figure 3.6.

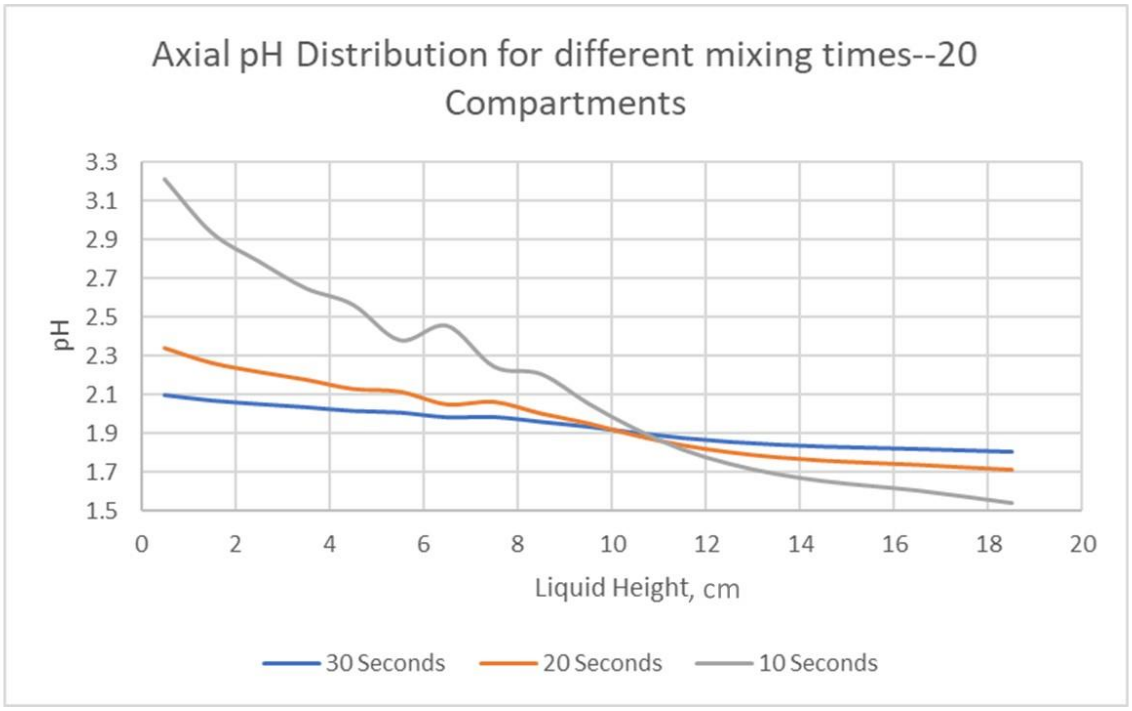

Figure 3.5. When the number of compartments is increased to 20, effecively increasing the model's resolution and dialing down the degree of ideal mixing, the total mixing time increases, and the pH distribution is more nuanced.

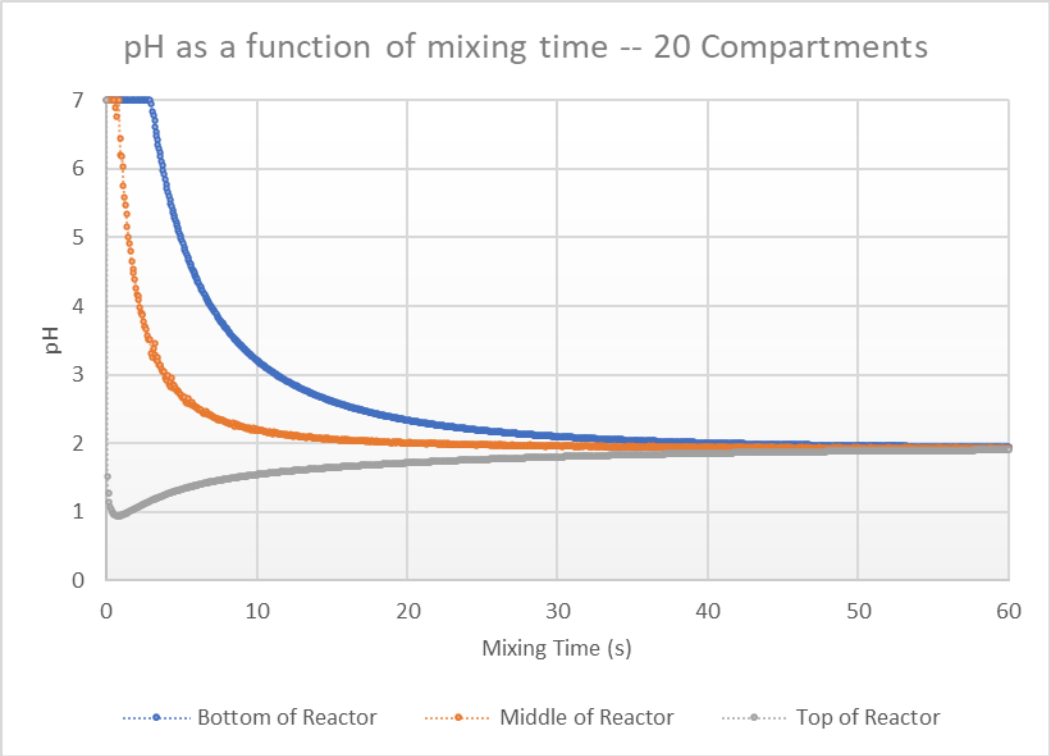

Figure 3.6. pH change across 60 seconds of mixing time for the 20-compartment model. Total mixing time is predicted to be greater, without complete homogeneity after 60 seconds.

The compartment models are compared in Figure 3.7 for mixing times of 30 seconds and 20 seconds. The disparity between the two models is most evident at shorter mixing times. With more significant volumes of idealized mixing space, it is to be expected that the 12-compartment model predicts shorter mixing times.

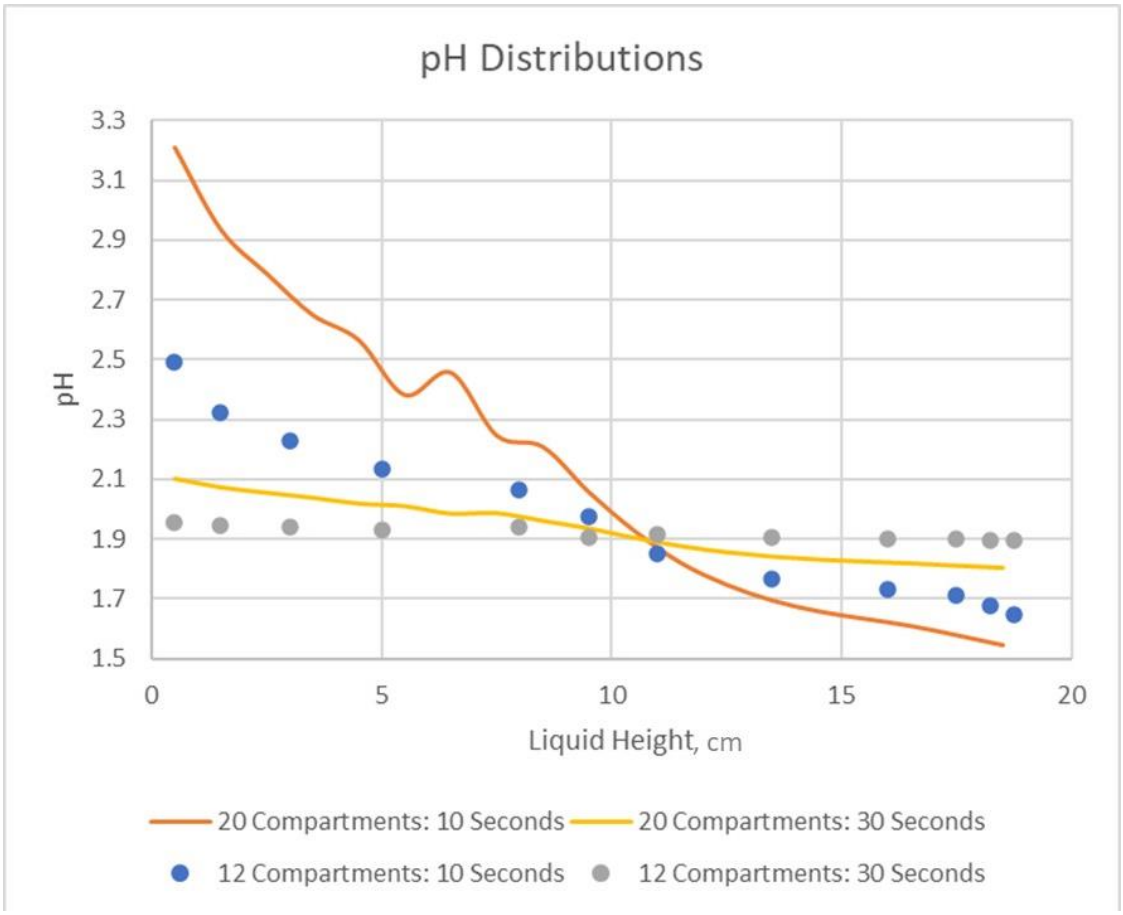

Figure 3.7. The pH distribution for 30 seconds and 10 seconds for each compartment model.

The 20-compartment model was compared to the CFD model in the same manner as the 12-compartment model. This is displayed graphically in Figure 3.8 and tabulated in Table 3.4. Comparison of the 20-compartment model and CFD model pH distribution after 60 seconds of mixing time at different axial positions.. The 20-compartment model shows much better agreement than the 12-compartment model. This is expected because as the number of compartments is increased, the model resolution moves closer to the CFD model. It should be noted, however, that for a simple mixing model that tracks concentration changes across the

reactor, this has no measurable effect on the computation time. As other parameters are incorporated, such as kinetics, energy balances for temperature prediction, air flow with bubble distribution, or any other considerations for the successful modeling of a bioreactor, the number of simultaneous ordinary differential equations will increase by a multiple of the number of compartments. Therefore, it is advantageous to eliminate compartments if possible, depending on the level of resolution needed for the modeling goal.

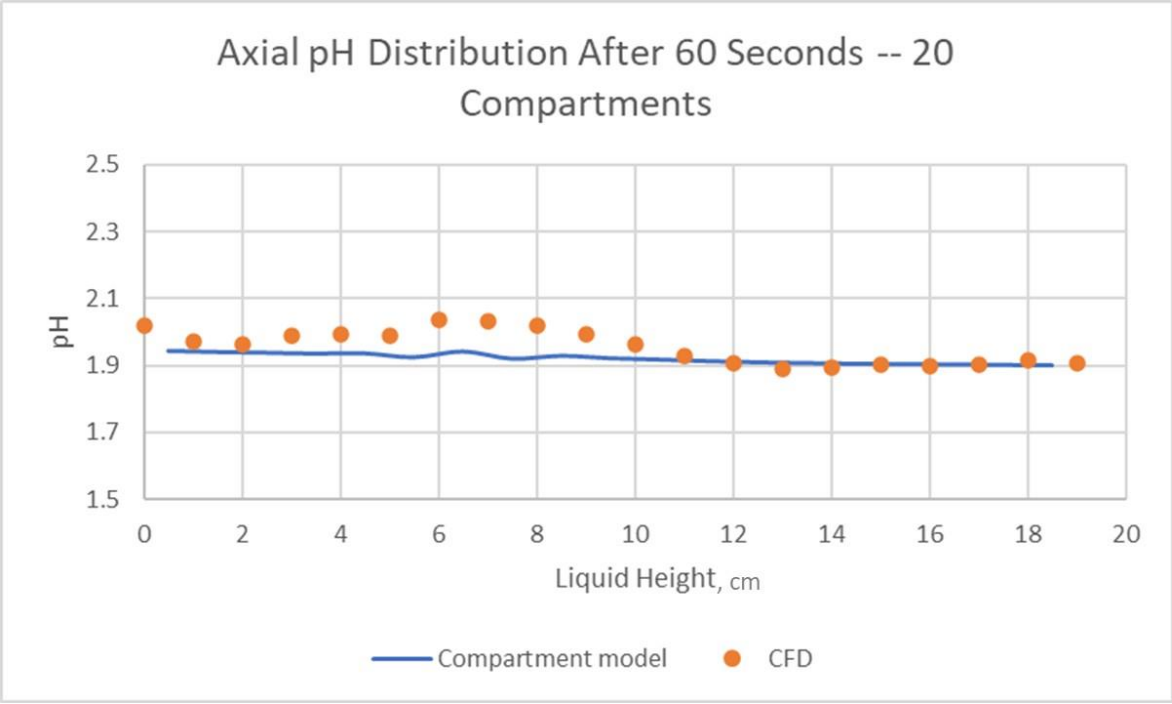

Figure 3.8. Comparison of the axial distribution of the 20-compartment model and the axial distribution of the pH of the CFD model.

Table 3.4. Comparison of the 20-compartment model and CFD model pH distribution after 60 seconds of mixing time at different axial positions.

Z	CFD-CM	CFD	%difference
0.5	1.94	2.00	2.70%
1.5	1.94	1.97	1.43%
2.5	1.94	1.98	1.94%
3.5	1.94	1.99	2.80%
4.5	1.94	1.99	2.76%
5.5	1.93	2.01	4.36%
6.5	1.94	2.03	4.68%
7.5	1.92	2.03	5.33%
8.5	1.93	2.01	3.87%
9.5	1.92	1.98	2.83%
10.5	1.925	1.95	1.46%
11.5	1.91	1.92	0.18%
12.5	1.91	1.90	0.72%
13.5	1.91	1.89	0.90%
14.5	1.91	1.90	0.43%
15.5	1.91	1.90	0.27%
16.5	1.91	1.90	0.22%
17.5	1.90	1.91	0.27%
18.5	1.90	1.91	0.46%

While the 60-second mixing profile showed good agreement for the 20-compartment model, prediction of the concentration profile at shorter time intervals proved less reliable. For the case of 30 seconds of mixing time, the error near the bottom of the reactor reached 50%, as demonstrated in Figure 3.9:

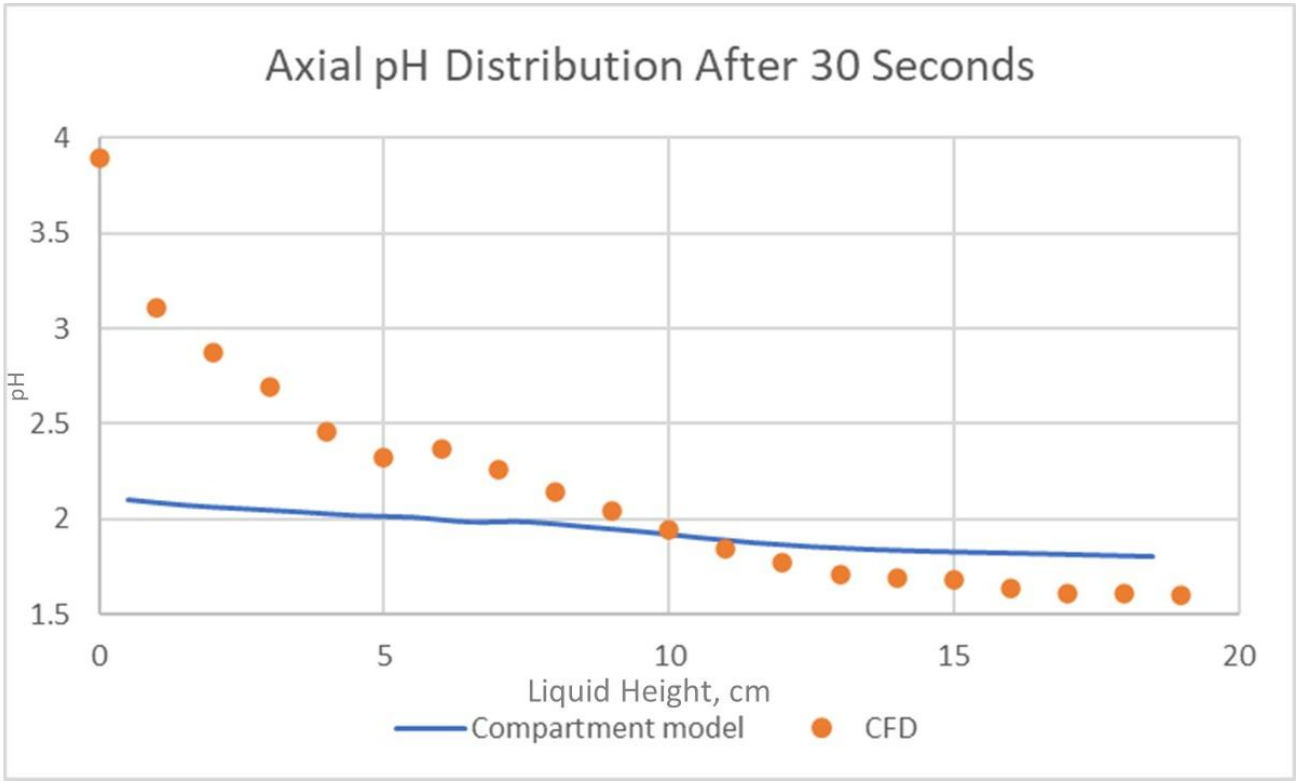

Figure 3.9. Comparison of the axial pH distrubtion predicted after 30 seconds of mixing time for the CFD model and the 20-compartment model.

While prediction is reasonable for the top half of the reactor, there is substantial divergence within the bottom half. Most likely, radial influences or other complex flow behavior becomes more prevalent as the fluid depth increases. If the parameter of interest is purely mixing time, then both models indicate that mixing has not yet been completed. However, it is clear that the CFD and CFD-CM models do not predict the same axial mixing rate. The CFD output is partitioned into more broad timesteps than those used by the CFD-CM. As a result, it is

challenging to make a direct comparison. However, the data has been superimposed inFigure 3.10:

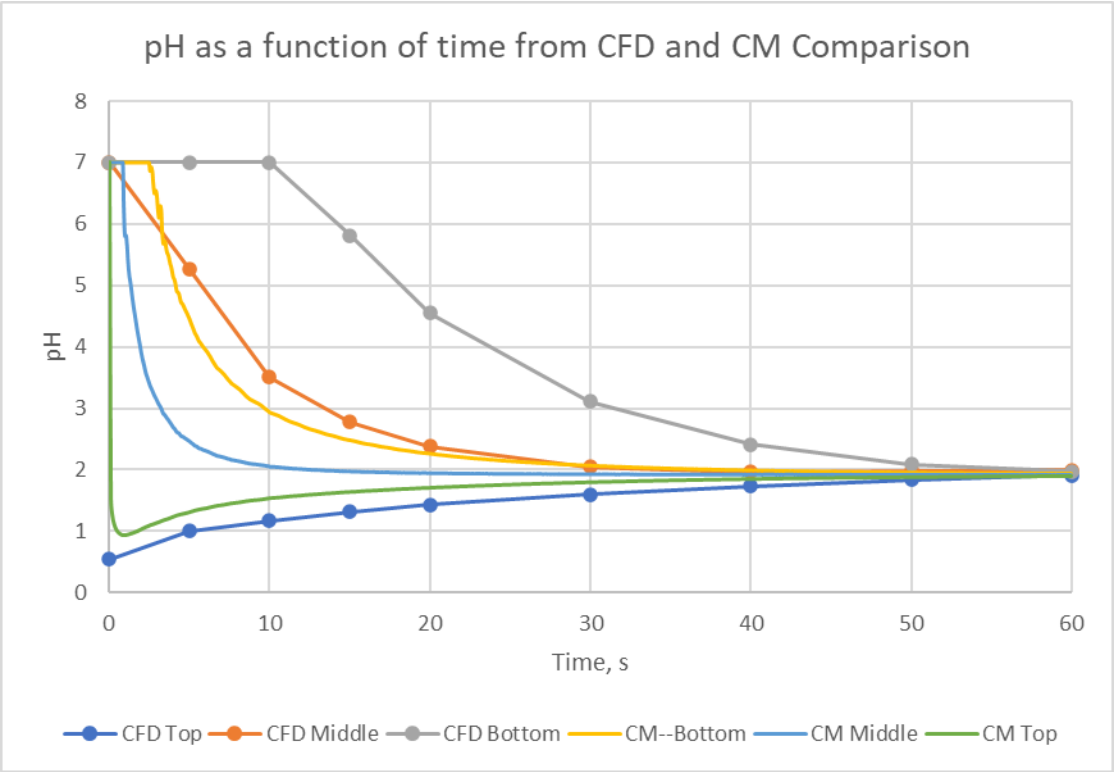

Figure 3.10. CFD and CM comparison of the pH evolution during a mixing time of 60 seconds.

The above figure shows that both models converge to a final mixing time of 60 seconds. However, there is a keen loss of fidelity in the 20-compartment model for lesser fluid heights across the entire time domain. This indicates that ignoring the radial effects of the fluid flow, particularly as reactor depth increases, may not be appropriate.

3.4 – Pulse Injection

A pulse injection was simulated to test model performance with a more realistic scenario. For acid injection into a real reactor, this will be performed through a specified diameter pipe at a predetermined flowrate. The CFD model rigorously accounts for the specific injection point by defining a boundary condition with a constant mass flux. However, the compartment model accounts for the injection by assuming an addition of a specified number of moles of acid per second into the top, ideally mixed, 1/2 cm of the reactor. The evolution of the pH across a 60-second mixing time for each compartment model is shown in Figure 3.11 and Figure 3.12.

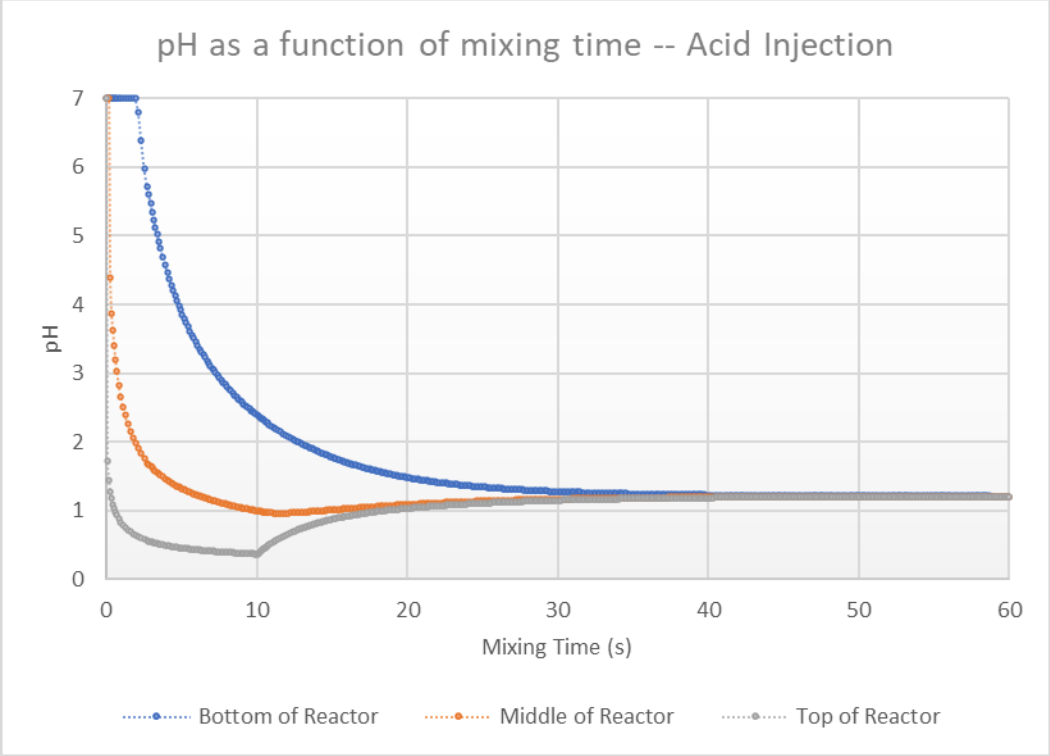

Figure 3.11. 12-compartment model simulation of acid injection. pH at different reactor heights over a mixing time of 60 seconds

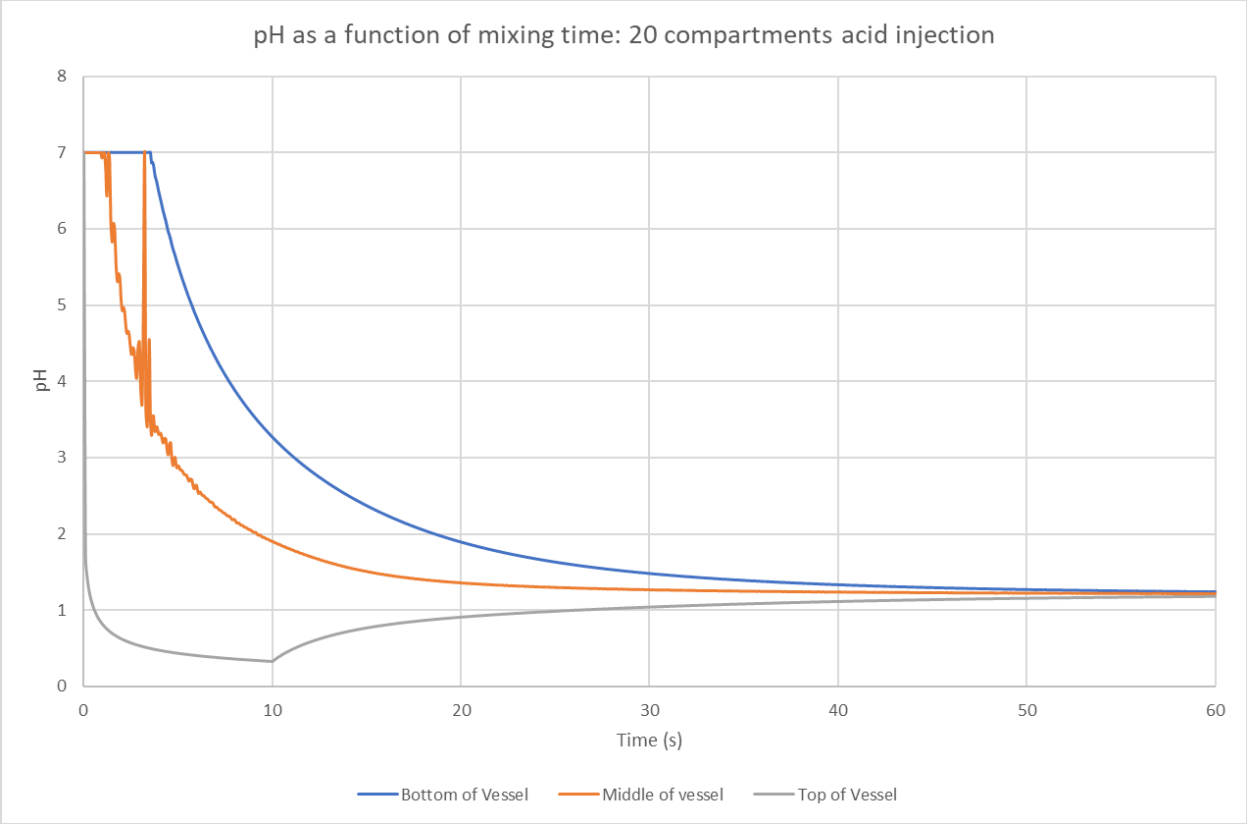

Figure 3.12. 20-compartment model simulation of acid injection. pH at different reactor heights over a mixing time of 60 seconds.

Compared to the 12-compartment model, the 20-compartment model shows signs of numerical instability at very short (less than 5 seconds) mixing times for the central compartments in the reactor. This is most likely an artifact of the perfect mixing assumption in compartments adjacent to high-velocity reactor zones and is in line with similar numerical issues encountered with shorter mixing times during the acid injection with the CFD model. The CFD model predicted nearly half of the zones to have a zero concentration after 30 seconds of mixing but achieved a resolved solution after 60 seconds. The pulse injection generates a larger overall acid concentration in the reactor due to the higher amount of acid. However, the concentration in the top of the creator gets much higher during the injection than in the initial condition model due to the unsteady-state molar balance for acid coming into the top compartment and acid

coming out of the compartment. There are no numerical issues following the acid injection during the mixing regime of the model. This suggests that, as predictive power increases for an axial compartment model, the generated information is more likely to contain numerical noise that interferes with a smooth solution. The CFD results for the injection were compared to both the 12-compartment and 20-compartment model, and those results are displayed in Figure 3.13 and Figure 3.14 with direct comparisons given in Table 3.5 and Table 3.6.

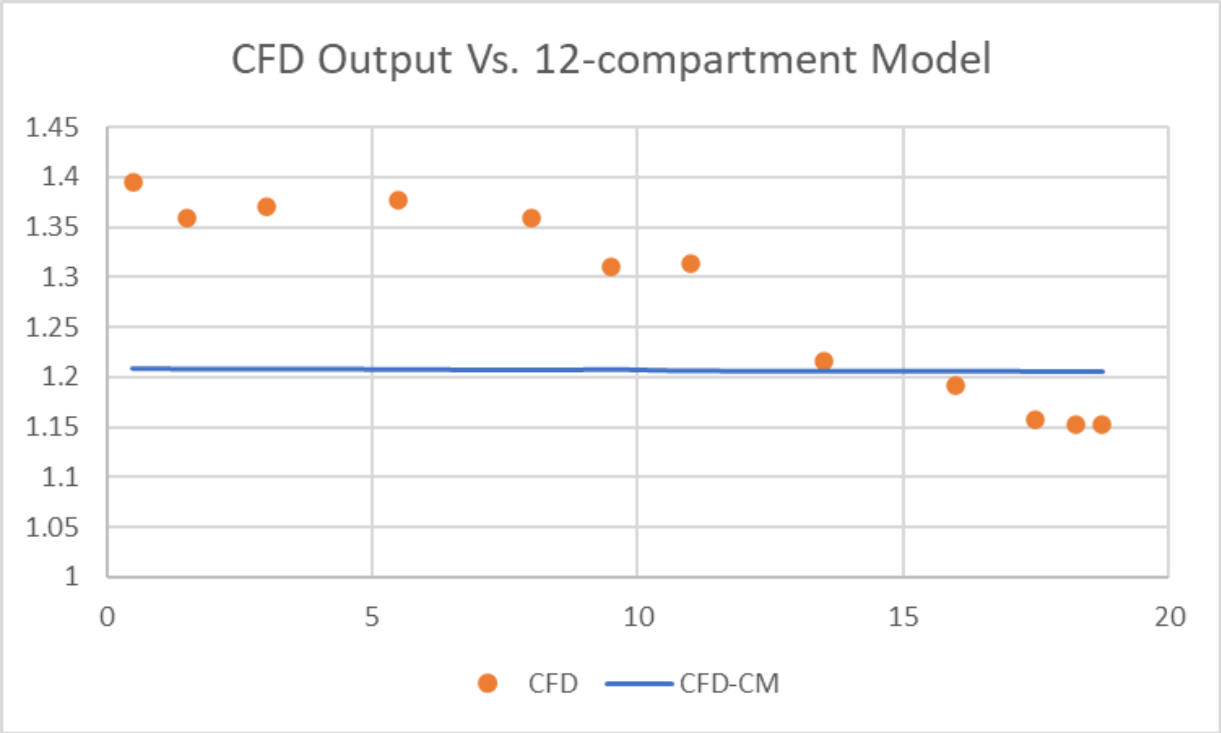

Figure 3.13. Comparison of CFD output and 12-compartment pH distribution after 60 seconds of mixing time.

Table 3.5. Comparison of CFD output and 12-compartment pH distribution after 60 seconds of mixing time.

Z (cm)	CFD-CM pH	CFD pH	%difference
0.5	1.21	1.39	14.24%
1.5	1.21	1.36	11.80%
3	1.21	1.37	12.55%
5.5	1.21	1.38	13.13%
8	1.21	1.36	11.79%
9.5	1.21	1.31	8.09%
11	1.21	1.31	8.50%
13.5	1.21	1.22	0.85%
16	1.21	1.19	1.24%
17.5	1.21	1.16	4.03%
18.25	1.21	1.15	4.48%
18.75	1.21	1.15	4.51%

While the 12-compartment model shows a well-mixed solution after 60 seconds, the CFD output predicts that mixing has not quite finished at this point. Compared to the initial condition case, the CFD-CM model with 12 compartments shows poor reproducibility with the CFD model. Because the initial condition case demonstrated a much better model fit, mixing effects local to the injection site in the vessel fluid likely play a more significant role in the overall mixing dynamics.

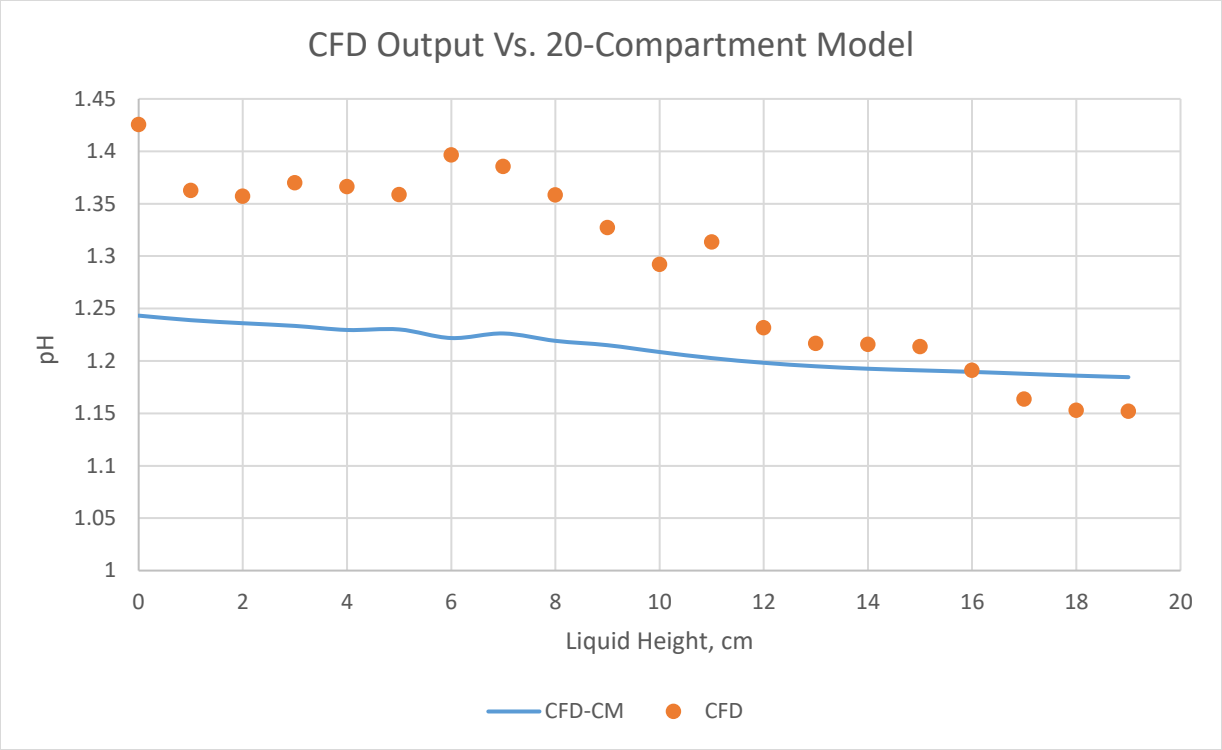

Figure 3.14. Comparison of the 20-compartment model with the CFD pH distribution after a mixing time of 60 seconds.

Table 3.6. Comparison of CFD output and 20-compartment pH distribution after 60 seconds of mixing time.

Z	CFD-CM	CFD	%difference
0	1.24	1.43	13.67%
1	1.24	1.36	9.53%
2	1.24	1.36	9.35%
3	1.23	1.37	10.49%
4	1.23	1.37	10.55%
5	1.23	1.36	9.95%
6	1.22	1.40	13.35%
7	1.23	1.39	12.20%
8	1.22	1.36	10.81%
9	1.22	1.33	8.83%
10	1.21	1.29	6.68%
11	1.20	1.31	8.82%
12	1.20	1.23	2.76%
13	1.19	1.22	1.82%
14	1.19	1.22	1.94%
15	1.19	1.21	1.89%
16	1.19	1.19	0.13%
17	1.19	1.16	2.06%
18	1.19	1.15	2.82%
19	1.18	1.15	2.77%

The 20-compartment model exhibits a similar degree of error with the pH distribution prediction after 60 seconds of mixing time. The overall model better fits the CFD data and predicts that mixing has not been completed after 60 seconds. However, the quantified error is still much greater than that predicted for the initial condition case.

A constant injection modeled using CFD most likely decreases the degree of radial homogeneity, rendering the perfect radial mixing assumption invalid. This is evidenced by the increased agreement between the CFD model and the 20-compartment model when compared to the 12-compartment model. As axial regions become smaller, the residence time in each compartment decreases. The average residence time decreased from 1.01 seconds in the 12-compartment model to 0.62 seconds in the 20-compartment model. It can be concluded, therefore, that the residence time threshold used by Bisgaard et al. may not be applicable to the case of a simulated acid injection. To more fully match the injection, a shorter residence is needed. This being said, the degree of error for the 20-compartment model is much greater for the injection case than for the initial condition case. It must be concluded, therefore, that radial mixing effects, similar to the volume of internal vessel components, have a marked effect on the mass transfer within the vessel, and cannot be reliably ignored in all cases for modeling purposes. However, the axial compartment model does show merit and exhibits good predictive power for overall vertical mixing effects within the vessel when initial conditions are matched between the CFD and CFD-CM models.

CHAPTER 4 - Discussion and Future Work

Reducing the total number of compartments from an initial amount helps to make the compartment generation process leverageable to larger-scale reactors. The method is also semi-automatic in that compartments are generated for the most part without intervention from the designer. The exception is the top and bottom compartments, which needed to tolerate a relaxation of the threshold residence time due to the no-slip top and bottom boundary conditions for flow in the CFD model. The modeling constraint of zero axial velocity at the fluid surface may cause the CFD model to underestimate the mixing time for compartments near Z = 19cm and Z =0cm. As a result of this modeling artifact, the residence time for the quasi-one-dimensional axial compartment model increases to infinity as compartments become smaller near the axial boundary conditions. Therefore, it was necessary to accept the tradeoff of reduced resolution in these locations to investigate a purely axial CM developed from CFD analysis. Accounting for the mixing behavior near the boundary conditions is a way to augment the axial CM is reserved for future work.

This model has the potential to predict process response to step changes from a steady-state operation. In particular, total mixing times can be predicted based on small fluid additions. However, a significant limitation exists in that it does not provide detailed information in the radial direction of the reactor. As a result, parameters such as heat input from the coils or the jacket cannot be rigorously modeled with this approach. It is possible, however, to predict the local axial concentrations of cells, substrate, and dissolved oxygen to arrive at a more detailed approximation of reactor performance. As an extension, an energy balance can be constructed for ambient cooling based on a heat loss coefficient from the reactor wall and the overall modeled mixing effects. To incorporate this into the compartment model, conductive and radiative heat

transfer effects could be ignored as a starting point. Instead, it can be assumed that energy is transferred internally entirely due to the motion of the fluid and convectively from the reactor walls. The fluid flowrate within the compartment, and either CFD modeling or empirical temperature measurements, can be used to determine the overall heat transfer coefficient as a function of axial volumetric flowrate. This can be incorporated into heat loss terms in each compartment to model position-based reactor cooling or heat gain terms based on available coil area and the local heat transfer coefficient.

The model also does not differentiate between a single phase and a two-phase flow regime. This can be incorporated, however, by utilizing the CFD results for the local average fraction of gas along the same axial positions as velocity. An average of the gas phase volume can then be taken, and a population balance model can be incorporated to track individual air bubbles in each compartment. Using the diffusivity of oxygen and the surface area of the bubble, the average oxygen concentration in each compartment can be calculated, yielding a steady-state dissolved oxygen axial gradient based on air flowrate. From CFD models developed using different air flowrates, a function can be developed so that the CFD-CM automatically adjusts exchange flows to account for velocity changes due to air injection.

Because the compartment model predicted faster mixing than the CFD model, incorporating the volume losses in the compartments based on the internal reactor components would have resulted in a broader prediction gap. This, and the wide disparity of predictive power between the initial condition case and the injection case, suggests that radial mixing effects play a nontrivial role in the total mixing effects in this particular reactor. Additional work can be conducted to investigate this hypothesis to characterize compartments within these axial zones to

produce a proper network. Because the initial condition cases showed good agreement, the focus should likely be on the boundary conditions or the injection site.

To truly evaluate the efficacy of the axial compartment model for use with a bioreactor, the concentration gradients and mixing assumptions must be validated using pH measurements in the physical bioreactor. Once this work is completed, radial mixing effects near injection points and boundary conditions can be explored to better fit the CFD-CM to the CFD simulation. In its current form, the model can rudimentarily predict total mixing time from an instantaneous acid addition, and refinement is needed to glean any useful information about the flow system. Among other things, radial effects must be considered throughout the reactor. By incorporating such horizontal compartments and possibly integrating portions of axial compartments, a network may be developed that more accurately characterizes the flow field and therefore is better able to match the dynamic response prediction of the CFD model.

The next step is to develop an energy balance and eventually incorporate the two-phase flow effects. It is likely possible to develop functions to describe how axial flowrates change based on the amount of air injection. Additionally, effects on impeller speed with axial and radial flowrates should be investigated to encompass the full scope of flow possibilities. Evaluating and refining the CFD-CM for these influences will lead to a better understanding and representation of the vessel behavior. The capstone for the CFD-CM digital twin development can therefore be modeling and validating a bioreaction, such as ethanol production.

Conclusions

An axial compartment model was developed from flow data generated via CFD analysis for a bench-scale bioreactor. The major benefit to this quasi one-dimensional model is the relatively cheap computation power required to obtain a solution. The compartmentalization strategy was initially adapted from a method to zone an ideal flow network based on empirical data [10]. However, it was determined that the assumption of a threshold residence time in each reactor of approximately 1 second is not generally applicable. Furthermore, when the compartment model was extended to include 20 compartments, much better agreement with the CFD results was observed.

The developed CFD-CM models were tested for a simulated acid addition step change. The CFD-CM requires an initial condition to be set for the concentration of each compartment. Therefore, the first comparison with the CFD output started with an initial condition of a homogenous pH region in the top ½ cm of the reactor. Both the 12-compartment model and the 20-compartment model reasonably matched the pH distribution predicted by the CFD model after 60 seconds of mixing time. However, the concentration distribution before a well-mixed state was not predicted, with errors reaching up to 50% when compared after 30 seconds of mixing. Furthermore, when the physical fluid injection was rigorously modeled using CFD, the compartment models did not match the CFD results. While promising, the model results demonstrate that further work is needed to refine this kind of CFD-CM to account for the internal volume of vessel components and radial mixing effects.

References

[1] C. Wittman, J. Liao, S. Lee, J. Nielsen and G. Stephanopoulos, Industrial Biotechnology: Products and Processes, John Wiley & Sons, Inc, 2017.

[2] M. Shuler, F. Kargi and M. DeLisa, Bioprocess Engineering: Basic Concepts, 3rd Ed., Prentice Hall, 2017.

[3] S. Enfors, M. Jahic, A. Rozkov, B. Xu, M. Hecker, B. Jurgen, E. Kruger, T. Schweder, G. Hamer, D. O'Beirne, N. Noisommit-Rizzi, M. Reuss, L. Boone, C. Hewitt, C. McFarlane, A. Nienow, T. Kovacs, C. Tragardh, L. Fuchs, J. Revsetedt, P. C. Friberg, B. Hjertager, G. Blomsten, H. Skogman, S. Hjort, F. Hoeks, H. Y. Lin, P. Neubaur, R. van der Lans, K. Luyben, P. Vrabel and A. Manelius, "Physiological Responses to mixing in large scale bioreactors," *Journal of Biotechnology,* vol. 85, no. 2, pp. 175 - 185, 2001.

[4] S. Fogler, Elements of Chemical Reaction Engineering, 5th ed, Prentice Hall, 2016.

[5] N. Jourdan, T. Neveux, O. Potier, M. Kanniche and W. J, "Compartmental Modelling in chemical engineering: A critical review," *Chemical engineering science,* no. 210, p. 115196, 2019.

[6] M. Pigou and J. Morchain, "Investigating the interactions between physical and biological heterogeneities in bioreactors using compartment, population balance, and metabolic models," *Chemical Engineering Science,* no. 126, pp. 267 - 282, 2015.

[7] Y. Tobo, J. Bartacek and I. Nopens, "Linking CFD and kinetic models in anaerobic digestion using a compartmental model approach," *Processes,* vol. 8, no. 703, 2020.

[8] G. Nadal-Rey, D. McClure, J. Kavanagh, B. Cassels, S. Cornelissen, D. Fletcher and K. Gernaey, "Development of dynamic compartment models for industrial aerobic fed-batch fermentation processes," *Chemical Engineering Journal,* no. 420, p. 130402, 2021.

[9] P. Vrabel, G. v. d. Lans, Y. Cui and K. Luyben, "Compartment Model Approach: Mixing in Large Scale Aerated Reactors with Multiple Impellers," *Trans IChemE,* no. 77, 1999.

[10] J. Bisgaard, T. Tajsoleiman, M. Muldbak, T. Tydal, T. Trasmussen, J. Huusom and K. Gernaey, "Automated compartment model development based on data from flow-following sensor devices," *Processes,* vol. 9, no. 1651, 2021.

[11] T. Tajsoleiman, R. Spann, C. Bach, K. Gernaey, J. K. Huusom and U. Kruhne, "A CFD based automatic method for compartment model development," *Computers and Chemical Engineering,* no. 123, pp. 236-245, 2019.

[12] J. Barneveld and W. Smit, "Measuring the liquid circulation time in a large gas-liquid contactor by means of a radio pill 1. Flow pattern and mean circulation time," *Chem. Res.,* no. 26, pp. 2185-2192, 1987.

[13] S. Reinecke, A. Deutschmann, K. Jobst, H. Kryk, E. Friedrich and U. Hampel, "Flow following sensor particles -- Validation and macro-mixing analysis in a stirred fermentation vessel with a highly viscous substrate," *Biochemical Engineering Journal,* no. 69, pp. 159-171, 2012.

[14] N. M. G. Oosterhuis and N. W. F. Kossen, "Dissolved Oxygen Concentration Profiles in a Production-Scale Bioreactor," *Biotechnology and Bioengineering,* vol. XXVI, pp. 546-550, 1984.

[15] J. Alvare and M. H. Al-Dahhan, "Liquid phase mixing in trayed bubble column reactors," *Chemical Engineering Science,* no. 61, pp. 1819-1835, 2006.

[16] A. Buss, A. Suleiko, K. Rugele and J. Vanags, "CFD Analysis of a stirred vessel bioreactor with double pitch blade and Rushton Type Impellers," in *COMSOL Conference in Rotterdam,* Rotterdam, 2017.

[17] L. Shu, M. Yang, H. Zhao, T. Li, L. Yang, X. Zou and Y. Li, "Process optimization of a stirred tank bioreactor based on CFD-Taguchi Method: A case study," *Journal of Cleaner Production,* no. 230, pp. 1074-1084, 2019.

[18] A. H. Alexopoulos, D. Maggioris and C. Kiparissides, "CFD analysis of turbulence non-homogeneity in mixing vessels A two-compartment model," *Chemical Engineering Science,* no. 57, pp. 1735-1752, 2002.

[19] D. Guha, M. P. Dudokovic and P. A. Ramachandran, "CFD-Based Compartment Modeling of single phase stirred-tank reactors," *AIChE Journal,* vol. 52, no. 5, 2006.

[20] F. Bezzo, S. Macchietto and C. C. Pantelides, "General Hybrid Multizonal/CFD approach for bioreactor modelling," *AICHe Journal,* vol. 49, no. 8, 2003.

[21] R. Spann, K. Gernaey and G. Sin, "A compartment model for risk-based monitoring of lactic acid bacteria cultivations," *Biochemical Engineering Journal,* no. 151, p. 107293, 2019.

[22] E. Nauha, Z. Kalal, J. M. Ali and V. Alopaeus, "Compartment modeling of large stirred tank bioreactors with high gas volume fractions," *Chemical Engineering Journal,* no. 334, pp. 2319-2334, 2018.

[23] Y. L. Moullec, C. Gentric, O. Potier and J. P. Leclerc, "Comparison of systemic, compartmental and CFD modelling approaches: application to the simulation of a biological reactor of wastewater treatment," *Chemical Engineering Science,* no. 65, pp. 343-350, 2010.

[24] A. Norregaard, C. Back, U. Kruhne, U. Borgbjerg and K. Gernaey, "Hypothesis-driven compartment model for stirred bioreactors utilizing computational fluid dynamics and multiple pH sensors," *Chemical Engineering Journal,* no. 356, pp. 161-169, 2019.

[25] F. Bezo, S. Maccietto and C. C. Pantelides, "A general methodology for hybrid multizonal/CFD models Part I. Theoretical Framework," *Computers and Chemical Engineering,* no. 28, pp. 501-511, 2004.

[26] F. Bezzo and S. Macchietto, "A general methodology for hybrid multizonal/CFD models Part II. Automatic zoning," *Computers and Chemical Engineering,* no. 28, pp. 513-525, 2004.

[27] A. Delafosse, M. Collignon, S. Calvo, F. Delvigne, M. Crine, P. Thonart and D. Toye, "CFD-based compartment model for description of mixing in bioreactors," *Chemical Engineering Science,* no. 106, pp. 76-85, 2014.

[28] C. Haringa, W. Tang and H. Noorman, "Stochasic parcel tracking in an Eurler-Lagrangle compartmnet model for fast simulation of fermentation processes," *Biotechnology Bioengineering,* no. 119, pp. 1849-1860, 2022.

[29] A. Krychowska, M. Kordas, M. Konopacki, B. Grygorcewicz, D. Musik, K. Wojcik, M. Jedrzejczak-silicka and R. Rakoczy, "Mathematical Modeling of Hydrodynamics in Bioreactor by Means of CFD-Based Compartment Model.," *Processes,* vol. 8, no. 1301, 2020.

[30] B. Weber, M. v. Campenhausen, T. Mabmann and A. Bednarz, "CFD based compartment-model for a multiphase loop-reactor," *Chemical Engineering Science,* vol. X, no. 2, p. 100010, 2019.

[31] M. Caramihai, I. Dumitrache and A. Chirvase, "Progress in characterization, modeling, and control of aerobic bioprocess Pt II: Aerobic bioprocess modeling and control," *Revue Roumaine de Chimie,* vol. 8, no. 54, pp. 619-635, 2009.

[32] Z. Duan, T. Wilms, P. Neubaur, C. Kravaris, M. Nicolas and M. Bournazou, "Model reduction of aerobic bioprocess models for efficient stimulation," *Chemical Engineering Science,* no. 217, p. 11512, 2020.

[33] M. Laakkonen, V. Alopaes and J. Aittamaa, "Validation of bubble breakage, coalescence and mass transfer models for gas-liquid dispersion in agitated vessel," *Chemical Engineering Science,* no. 61, pp. 218-228, 2006.

[34] M. Laakonen, P. Moilanen, V. Alopaeus and J. Aittaman, "Modelling local bubble size distributions in agitated vessels," *Chemical Engineering Science,* no. 62, pp. 721-740, 2007.

[35] V. Alopaeus, J. Koskinen, K. I. Keskinen and J. Majander, "Simulation of the population balances for liquid-liquid systems in a nonideal stirred tank. Part 2 -- Parameter fitting and the sue of the multiblock model for dense dispersions," *Chemical Engineering Science,* no. 57, pp. 1815-1825, 2002.

[36] M. J. Prince and H. W. Blanch, "Bubble coalescence and break-up in air-sparged bubble columns," *AIChE Journal,* no. 36, pp. 1485-1499, 1990.

[37] J. Gimbun, S. Y. Liew, Z. K. Nagy and C. D. Rielly, "Three-way coupling simulation of a gas-liquid stirred tank using a multi-compartment population balance model," *Chemical Product and Process Modeling,* vol. 11, no. 3, pp. 205-216, 2016.

Appendix A - Matlab Codes

```
function f = simul_diff(t,y)

%12 compartment model for initial condition case

%Volumetric Flowrates
Q1= 120.6006;
Q2= 337.3812;
Q3= 537.924;
Q4=940.6753;
Q5=787.0405;
Q6=430.7425;
Q7=497.4379;
Q8=823.0608;
Q9=667.8225;
Q10=243.5677;
Q11=154.7407;
Q12=77.37034;

%Compartment Volumes
V1=254.469;
V2=254.469;
V3=508.938;
V4=763.407;
V5=508.938;
V6=254.469;
V7=508.938;
V8=763.407;
V9=508.938;
V10=254.469;
V11=127.2345;
V12=127.2345;

f(1,1) = ((y(2)*Q1 - y(1)*Q1)/V1);
f(2,1) = ((Q1*y(1) + Q2*y(3) - y(2)*Q1 - y(2)*Q2)/V2);
f(3,1) = ((Q2*y(2) + Q3*y(4) - y(3)*Q2 -y(3)*Q3)/V3);
f(4,1) = ((Q3*y(3) + Q4*y(5) - y(4)*Q3 -y(4)*Q4)/V4);
f(5,1) = ((Q4*y(4) + Q5*y(6) - y(5)*Q4 -y(5)*Q5)/V5);
f(6,1) = ((Q5*y(5) + Q6*y(7) - y(6)*Q5 - y(6)*Q6)/V6);
f(7,1) = ((Q6*y(6) + Q7*y(8) - y(7)*Q6 - y(7)*Q7)/V7);
f(8,1) = ((Q7*y(7) + Q8*y(9) - y(8)*Q7 - y(8)*Q8)/V8);
f(9,1) = ((Q8*y(8) + Q9*y(10) - y(9)*Q8 - y(9)*Q9)/V9);
f(10,1) = ((Q9*y(9) + Q10*y(11) - y(10)*Q9 - y(10)*Q10)/V10);
f(11,1) = (Q10*y(10) + Q11*y(12) - y(11)*Q10 -  y(11)*Q11)/V11;
f(12,1) = ((Q11*y(11) - Q11*y(12))/V12);
end
```

```
function f = tight_threshold(t,y)
%20 compartment model initial condition case
%Volumetric Flowrates
Q1= 120.6006;
Q2= 337.3812;
Q3= 486.8381;
Q4=590.1054;
Q5=742.558;
Q6=1062.571;
Q7=1138.793;
Q8=787.0405;
Q9=515.9845;
Q10=430.7425;
Q11=447.5205;
Q12=543.0901;
Q13=653.0412;
Q14=807.6523;
Q15=993.0804;
Q16=835.5364;
Q17=461.9008;
Q18=243.5677;
Q19=154.7407;

%Compartment Volumes
V1=254.469;
V2 = 127.2345;

f(1,1) = ((y(2)*Q1 - y(1)*Q1)/V1);
f(2,1) = ((Q1*y(1) + Q2*y(3) - y(2)*Q1 - y(2)*Q2)/V1);
f(3,1) = ((Q2*y(2) + Q3*y(4) - y(3)*Q2 -y(3)*Q3)/V1);
f(4,1) = ((Q3*y(3) + Q4*y(5) - y(4)*Q3 -y(4)*Q4)/V1);
f(5,1) = ((Q4*y(4) + Q5*y(6) - y(5)*Q4 -y(5)*Q5)/V1);
f(6,1) = ((Q5*y(5) + Q6*y(7) - y(6)*Q5 - y(6)*Q6)/V1);
f(7,1) = ((Q6*y(6) + Q7*y(8) - y(7)*Q6 - y(7)*Q7)/V1);
f(8,1) = ((Q7*y(7) + Q8*y(9) - y(8)*Q7 - y(8)*Q8)/V1);
f(9,1) = ((Q8*y(8) + Q9*y(10) - y(9)*Q8 - y(9)*Q9)/V1);
f(10,1) = ((Q9*y(9) + Q10*y(11) - y(10)*Q9 - y(10)*Q10)/V1);
f(11,1) = (Q10*y(10) + Q11*y(12) - y(11)*Q10 -  y(11)*Q11)/V1;
f(12,1) = (Q11*y(11) + Q12*y(13) - y(12)*Q11 -  y(12)*Q12)/V1;
f(13,1) = (Q12*y(12) + Q13*y(14) - y(13)*Q12 -  y(13)*Q13)/V1;
f(14,1) = (Q13*y(13) + Q14*y(15) - y(14)*Q13 -  y(14)*Q14)/V1;
f(15,1) = (Q14*y(14) + Q15*y(16) - y(15)*Q14 -  y(15)*Q15)/V1;
f(16,1) = (Q15*y(15) + Q16*y(17) - y(16)*Q15 -  y(16)*Q16)/V1;
f(17,1) = (Q16*y(16) + Q17*y(18) - y(17)*Q16 -  y(17)*Q17)/V1;
f(18,1) = (Q17*y(17) + Q18*y(19) - y(18)*Q17 -  y(18)*Q18)/V1;
f(19,1) = (Q18*y(18) + Q19*y(20) - y(19)*Q18 -  y(19)*Q19)/V2;
f(20,1) = ((Q19*y(19) - Q19*y(20))/V2);
end
```

```
function f = Injection_pulse(t,y)
%injection pulse section of code. Run this code, then use the time at 10
%seconds as the initial conditions for the simul_diff function.
%Volumetric Flowrates
Q1= 120.6006;
Q2= 337.3812;
Q3= 537.924;
Q4=940.6753;
Q5=787.0405;
Q6=430.7425;
Q7=497.4379;
Q8=823.0608;
Q9=667.8225;
Q10=243.5677;
Q11=154.7407;
Q12=77.37034;

%Compartment Volumes
V1=254.469;
V2=254.469;
V3=508.938;
V4=763.407;
V5=508.938;
V6=254.469;
V7=508.938;
V8=763.407;
V9=508.938;
V10=254.469;
V11=127.2345;
V12=127.2345;

f(1,1) = ((y(2)*Q1 - y(1)*Q1)/V1);
f(2,1) = ((Q1*y(1) + Q2*y(3) - y(2)*Q1 - y(2)*Q2)/V2);
f(3,1) = ((Q2*y(2) + Q3*y(4) - y(3)*Q2 -y(3)*Q3)/V3);
f(4,1) = ((Q3*y(3) + Q4*y(5) - y(4)*Q3 -y(4)*Q4)/V4);
f(5,1) = ((Q4*y(4) + Q5*y(6) - y(5)*Q4 -y(5)*Q5)/V5);
f(6,1) = ((Q5*y(5) + Q6*y(7) - y(6)*Q5 - y(6)*Q6)/V6);
f(7,1) = ((Q6*y(6) + Q7*y(8) - y(7)*Q6 - y(7)*Q7)/V7);
f(8,1) = ((Q7*y(7) + Q8*y(9) - y(8)*Q7 - y(8)*Q8)/V8);
f(9,1) = ((Q8*y(8) + Q9*y(10) - y(9)*Q8 - y(9)*Q9)/V9);
f(10,1) = ((Q9*y(9) + Q10*y(11) - y(10)*Q9 - y(10)*Q10)/V10);
f(11,1) = (Q10*y(10) + Q11*y(12) - y(11)*Q10 -  y(11)*Q11)/V11;
f(12,1) = ((Q11*y(11) - Q11*y(12) + 0.029646)/V12);
% The constant in equation 12 simulates an addition of 1mL per second of 98% sulfuric acid to the
top of the reactor. this is 0.0184 mol/s of H2SO4, or 0.0368 mol/s of H+.
% This is a smoothed addition of the CFD injection pulse, that has been
% corrected for the bulk volume difference between the CFD reactor and the
% CM reactor. This volume difference can also be corrected in the
```

```
% compartment formulation stage of the model development procedure.
End
```

```
function f = injection_20CM(t,y)
%injection case for 20-compartment model. use output of this function at 10
%seconds as initial conditions for tight_threshold function
%Volumetric Flowrates
Q1= 120.6006;
Q2= 337.3812;
Q3= 486.8381;
Q4=590.1054;
Q5=742.558;
Q6=1062.571;
Q7=1138.793;
Q8=787.0405;
Q9=515.9845;
Q10=430.7425;
Q11=447.5205;
Q12=543.0901;
Q13=653.0412;
Q14=807.6523;
Q15=993.0804;
Q16=835.5364;
Q17=461.9008;
Q18=243.5677;
Q19=154.7407;

%Compartment Volumes
V1=254.469;
V2 = 127.2345;

f(1,1) = ((y(2)*Q1 - y(1)*Q1)/V1);
f(2,1) = ((Q1*y(1) + Q2*y(3) - y(2)*Q1 - y(2)*Q2)/V1);
f(3,1) = ((Q2*y(2) + Q3*y(4) - y(3)*Q2 -y(3)*Q3)/V1);
f(4,1) = ((Q3*y(3) + Q4*y(5) - y(4)*Q3 -y(4)*Q4)/V1);
f(5,1) = ((Q4*y(4) + Q5*y(6) - y(5)*Q4 -y(5)*Q5)/V1);
f(6,1) = ((Q5*y(5) + Q6*y(7) - y(6)*Q5 - y(6)*Q6)/V1);
f(7,1) = ((Q6*y(6) + Q7*y(8) - y(7)*Q6 - y(7)*Q7)/V1);
f(8,1) = ((Q7*y(7) + Q8*y(9) - y(8)*Q7 - y(8)*Q8)/V1);
f(9,1) = ((Q8*y(8) + Q9*y(10) - y(9)*Q8 - y(9)*Q9)/V1);
f(10,1) = ((Q9*y(9) + Q10*y(11) - y(10)*Q9 - y(10)*Q10)/V1);
f(11,1) = (Q10*y(10) + Q11*y(12) - y(11)*Q10 -  y(11)*Q11)/V1;
f(12,1) = (Q11*y(11) + Q12*y(13) - y(12)*Q11 -  y(12)*Q12)/V1;
f(13,1) = (Q12*y(12) + Q13*y(14) - y(13)*Q12 -  y(13)*Q13)/V1;
f(14,1) = (Q13*y(13) + Q14*y(15) - y(14)*Q13 -  y(14)*Q14)/V1;
f(15,1) = (Q14*y(14) + Q15*y(16) - y(15)*Q14 -  y(15)*Q15)/V1;
f(16,1) = (Q15*y(15) + Q16*y(17) - y(16)*Q15 -  y(16)*Q16)/V1;
f(17,1) = (Q16*y(16) + Q17*y(18) - y(17)*Q16 -  y(17)*Q17)/V1;
f(18,1) = (Q17*y(17) + Q18*y(19) - y(18)*Q17 -  y(18)*Q18)/V1;
f(19,1) = (Q18*y(18) + Q19*y(20) - y(19)*Q18 -  y(19)*Q19)/V2;
f(20,1) = ((Q19*y(19) - Q19*y(20)+0.029646)/V2);
```

```
end
```